

Phase stability, point defects, and elastic properties of W-V and W-Ta alloysM. Muzyk,¹ D. Nguyen-Manh,^{2,*} K. J. Kurzydłowski,¹ N. L. Baluc,³ and S. L. Dudarev²¹*Materials Design Division, Faculty of Materials Science and Engineering, Warsaw University of Technology, Wólowska 141, PL-02-507 Warsaw, Poland*²*EURATOM/CCFE Fusion Association, Culham Centre for Fusion Energy, Abingdon, Oxfordshire OX14 3DB, United Kingdom*³*Centre de Recherches en Physique des Plasmas, Association EURATOM - Swiss Confédération, École Polytechnique Fédérale de Lausanne, ODGA-C110, CH-5232 Villigen PSI, Switzerland*

(Received 28 March 2011; revised manuscript received 29 June 2011; published 12 September 2011)

The structure and phase stability of binary tungsten-vanadium and tungsten-tantalum alloys are investigated over a broad range of alloy compositions using *ab initio* and cluster expansion methods. The alloys are characterized by the negative enthalpy of mixing across the entire composition range. Complex intermetallic compounds are predicted by *ab initio* calculations as the lowest energy structures for both alloys. The effect of atomic relaxation on the enthalpy of mixing is almost negligible in W-V, but is substantial in W-Ta alloys. Canonical Monte Carlo simulations are used for predicting the order-disorder transition temperatures for both alloys. Differences in the short-range order between the two alloys are explained by the opposite signs of the second nearest-neighbour cluster interaction coefficients for W-V and W-Ta. Using the predicted ground-state structures, we evaluate the monovacancy formation energies and show that in W-Ta alloys they are highly sensitive to the alloy composition and the local environment of a vacancy site, varying from 3 to 5 eV. In the dilute tungsten alloy limit, a $\langle 111 \rangle$ self-interstitial atom crowdion defect forms a configuration strongly bound to a vanadium solute atom, whereas interaction between the same defect and a tantalum solute atom is repulsive. Values of elastic constants computed for all the ground-state structures and several metastable cubic alloy structures are used for assessing the effect of alloying on mechanical properties. Values of the Young modulus and the Poisson ratio, as well as the empirical Rice-Thompson criterion, are applied to screening the alloys, to assess the effect of chemical composition on ductility.

DOI: [10.1103/PhysRevB.84.104115](https://doi.org/10.1103/PhysRevB.84.104115)

PACS number(s): 61.72.jj, 62.20.de, 64.60.Cn, 71.15.Mb

I. INTRODUCTION

Tungsten has attractive engineering properties, including its high melting temperature, significant high-temperature strength, good thermal conductivity, and low sputtering rate, which make it suitable for various high-temperature applications including filament manufacturing. Recently, tungsten received attention as a candidate material for fusion power-plant technology, for example plasma-facing armour or shielding components, and some structural applications.¹⁻⁴ An armor material is expected to retain high fracture toughness under extreme thermal operating conditions, and it is also expected to be compatible with constraints derived from plasma-wall interaction studies.^{5,6} The drawbacks associated with technological applications of tungsten include its high brittle to ductile transition temperature (BDTT),⁷ significant irradiation embrittlement occurring even if the material is irradiated at relatively high temperatures, and the grain growth and recrystallization effects detrimental to its high-temperature performance,⁸ which together represent a major challenge for fusion materials science.⁹

A possible way of overcoming the problem of low-temperature brittleness of W, and improving its recrystallization behavior and radiation stability, consists of the identification of alloying elements increasing the ductility of the material. For example, rhenium reduces the BDTT and increases both ductility and hardness of tungsten.¹⁰⁻¹³ At the same time, alloying W with Re reduces radiation swelling of tungsten.¹⁴ Of further significance for the design of W components for fusion power generation is the effect of nuclear

transmutations.¹⁵⁻¹⁷ The primary products of neutron-induced nuclear transmutations of tungsten are rhenium and osmium. Calculations by Cottrell¹⁷ suggest that after five years of exposure to fusion neutrons, the concentration of Re in W may reach 11.8 at. %, whereas Os concentration may reach 12.7 at. %. This would give rise to the formation of ternary alloys W-Re-Os in the composition range close to that of the σ phase. The formation of σ -phase precipitates, which are both denser and more brittle than the original body-centred-cubic (bcc) α -phase crystal structure, would have a detrimental effect on mechanical properties. However, a recent study by Gilbert and Sublet,¹⁸ which takes into account the effect of giant resonances in the absorption nuclear scattering cross section on the neutron energy spectrum and nuclear transmutation rates, shows that after five years of fusion neutron irradiation the concentration of rhenium reaches only 3.8 at. %, whereas the osmium concentration remains below 1.4 at. %. These results suggest that the formation of σ -phase precipitates in tungsten under fusion neutron irradiation is less likely than was previously anticipated.

In this paper we describe results of an *ab initio* study of phase stability and elastic constants of binary W-V and W-Ta alloys. The experimental phase diagrams of W-Ta and W-V alloys are given in Refs. 19-21. These phase diagrams show that W-Ta and W-V alloys exhibit full solubility in bcc α phase up to the solidus line, showing no occurrence of intermetallic phases. Still, there are indications that chemical short-range order (SRO) is present in these systems. Experimental results show that solid W-Ta alloys exhibit deviations from the ideal solid solution behavior over the temperature range between

1050 and 1200 K.²² Furthermore, the measured negative excess free energies of mixing result primarily from the negative enthalpies of mixing, and the observed small negative entropies of mixing can be attributed to phonon excitations. First-principles electronic structure calculations were carried out recently to investigate the negative enthalpies of mixing of W-Ta alloys,^{23–25} whereas theoretical analysis of phase stability of W-V alloys is almost absent in the literature. The enthalpies of mixing of binary W-V alloys calculated using an effective pair interaction model²⁶ or tight-binding electronic structure methods²⁷ were found to be positive, at variance with experimental observations showing negative deviations from Vegard’s law.¹⁹ The observed negative enthalpies of mixing suggest the occurrence of chemical ordering, but none has yet been found experimentally in the range of temperatures accessible to observations. This can be explained by the exceedingly slow self-diffusion in the alloys and the resulting long structure relaxation time scales. The latter is consistent with our earlier first-principles calculations showing high vacancy formation ($\simeq 3.5$ eV) and vacancy migration ($\simeq 1.8$ eV) energies in bcc tungsten.^{28–30} The fact that time scales associated with processes controlled by diffusion of vacancies in tungsten, for example those involved in the formation of dislocation loops in collision cascades, are significantly greater than in other metals is consistent with *in situ* electron microscope observations of microstructural evolution under irradiation.³¹ Binding energies of complexes involving interstitial impurity atoms, for example carbon or nitrogen, and vacancies, are also higher in tungsten in comparison with other bcc transition metals.³²

Our study is a part of a broader program of work aimed at finding out how the choice of chemical composition and microstructure influences properties of materials exposed to fusion neutron irradiation. Using *ab initio* calculations, we attempt to rationalize systematic trends characterizing phase stability, point defects, and elastic properties of concentrated W-Ta and W-V binary alloys, as a step toward modeling larger-scale microstructural features including grain boundaries, dislocations, and dislocation ensembles. The stability of microstructure in the environment of a fusion power plant, where the combined effect of high temperature, stresses, and irradiation drives nonequilibrium microstructural evolution, determines engineering properties of materials.³³ *Ab initio* calculations provide information about microscopic phenomena, the understanding of which is required for the development of larger-scale coarse-grained models, for example molecular dynamics and Monte Carlo simulations. *Ab initio* calculations also provide input for models describing fracture of tungsten-vanadium and tungsten-tantalum alloys.^{34,35}

The paper is organized as follows. In Sec. II, we describe a computational model for predicting low-energy phases of W-Ta and W-V binary alloys. The model combines *ab initio* and cluster expansion (CE) calculations. Using *ab initio* data, we deduce numerical values of CE interaction parameters for both W-Ta and W-V alloys. In Sec. III we investigate both the finite temperature thermodynamic properties and SRO of the alloys. These properties are calculated using canonical Monte Carlo simulations performed at fixed alloy compositions. Microstructural evolution of materials under irradiation is driven by accumulation, migration, and agglomeration of point

defects (vacancies and self-interstitial atoms), as well as by interaction of these defects with solute and impurity atoms in the alloys. In Sec. IV, we investigate the composition dependence of monovacancy formation energies, using the lowest energy structures of W-Ta and W-V alloys. A study of elastic constants spanning all the low-energy crystal structures is described in Sec. V. In the same section, we discuss implications of our findings for the fracture properties of the alloys. Section VI summarizes the results and concludes the paper.

II. GROUND-STATE PREDICTION

To predict the low-temperature structure of a binary alloy and investigate its phase stability at a finite temperature, we combine quantum-mechanical density-functional theory (DFT) calculations with lattice statistical mechanics simulation methods. We evaluate thermodynamic parameters characterizing the alloys, for example their enthalpies of mixing,

$$\Delta H_{\text{DFT}}(\vec{\sigma}) = E_{\text{tot}}(A_x B_{1-x}, \vec{\sigma}) - x E_{\text{tot}}(A) - (1-x) E_{\text{tot}}(B), \quad (1)$$

where x denotes the average concentration of component A of the alloy, and $1-x$ refers to the concentration of component B of the alloy. We use the lattice site occupation variables $\sigma_i = \pm 1$, which show whether a site i is occupied by an atom of type A (corresponding to $\sigma_i = +1$) or B (corresponding to $\sigma_i = -1$). If we denote by $\vec{\sigma}$ the vector of all the “spins” $\{\sigma_i\} = (\sigma_1, \sigma_2, \dots, \sigma_N)$, the configuration enthalpy of formation $\Delta H_{\text{DFT}}(\vec{\sigma})$ of the alloy is described exactly by a set of multisite interaction parameters $\{J\}$ entering an Ising-like Hamiltonian of the form

$$\Delta H_{\text{DFT}}(\vec{\sigma}) = J_0 + \sum_i J_i \sigma_i + \sum_{i,j} J_{i,j} \sigma_i \sigma_j + \sum_{i,j,k} J_{i,j,k} \sigma_i \sigma_j \sigma_k + \dots \quad (2)$$

This is the defining equation of the CE formalism.^{36–38} For a binary alloy $A_x B_{1-x}$, modeled using a cell with N sites, there are 2^N possible structures, each characterized by its own vector $\vec{\sigma}$. Attempting to perform *ab initio* calculations for all the 2^N transpositions of atoms in an alloy to find the minimum-energy structure is practically impossible. Hence Eq. (2) is often approximated by a CE Hamiltonian, expressed as a polynomial function of occupation variables,

$$\Delta H_{\text{CE}}(\vec{\sigma}) = \sum_{\alpha} m_{\alpha} J_{\alpha} \left\langle \prod_{i \in \alpha'} \sigma_i \right\rangle, \quad (3)$$

where α denotes a cluster (a set of sites i). Summation in Eq. (3) is over all the clusters α that are not equivalent to each other via a symmetry operation of the parent lattice space group, while the average is taken over all the clusters α' that are equivalent to α by symmetry. Coefficients J_{α} in this expansion embody information about the relative energies of alloy configurations, and are called the effective cluster interaction (ECI) parameters. Multiplicity m_{α} is the number of clusters equivalent by symmetry to α . In a real alloy, small

differences between atomic radii give rise to local distortions of the lattice. However, this does not change the topology of the crystal structure, and hence the cluster coefficients effectively map the actual relaxed distorted atomic lattice configurations onto a perfect lattice. In this way small local elastic deformations associated with atomic size mismatch are included in the cluster expansion coefficients. Alternatively, elastic effects can be taken into account explicitly using the method developed in Ref. 37.

Although Eq. (3) contains many ECIs J_α , the energy of interatomic bonds is usually dominated by short-range interactions. Therefore a relatively small number of parameters J_α already provides a sufficiently accurate mapping of DFT to CE. We note here that the accuracy of CE parametrization is not determined solely by the error in the energies predicted by CE in comparison with energies predicted by DFT. It is important to make sure that the CE model predicts the correct lowest energy crystal structures. In this paper we use the Alloy Theoretic Automatic Toolkit (ATAT),³⁹ which allows assigning extra weights to certain crystal structures, to ensure that the lowest energy structures predicted by CE simulations agree with DFT results.

To find the optimum set of ECIs for both W-Ta and W-V alloys, we use a database of DFT energies computed for 58 bcc-like structures. DFT calculations involve full atomic relaxations, as in our earlier studies of Fe-Cr binary alloys.^{40–42} Most of the DFT calculations described in this paper were performed using the Perdew-Burke-Ernzerhof electron exchange-correlation functional within generalized gradient approximation (PBE-GGA).⁴³ We used the projector augmented wave (PAW) pseudopotentials implemented in the Vienna Ab-initio Simulation Package (VASP).^{44–46} Given the fact that the semicore electronic states make a non-negligible contribution to the formation energies of self-interstitial atom (SIA) defects,^{28–30} all the calculations described in this work were performed using the PAW potentials X_{pv} , where the semicore p states are treated as valence states. The calculations were performed using a $4 \times 4 \times 4$ bcc supercell, with plane-wave cutoff energy of 400 eV and $3 \times 3 \times 3$ k -point mesh with spacing of 0.2 \AA^{-1} . In the case of pure bcc tungsten with two atoms per unit cell we used a $14 \times 14 \times 14$ k -point grid, corresponding to the same k -point spacing of 0.2 \AA^{-1} .

The calculated enthalpies of mixing for 58 crystal structures of W-Ta and W-V alloys are shown in Figs. 1 and 2, respectively, where they are labeled “DFT-Initial.” These initial input data include not only the conventional A_3B , AB_3 (DO_3), A_2B , AB_2 ($C11_b$), and AB (B_2) structures,²³ but also a number of $2 \times 2 \times 2$ bcc supercell structures, including $A_{15}B$ and AB_{15} , which span a broad range of alloy environments characterized by higher-order multiatom interactions. The enthalpies of mixing computed for the initial structures are negative for both alloys.

From the available DFT structure database, the initial values of CE interaction coefficients are derived using the so-called structure inversion method (SIM), also known as the Connolly-Williams method.⁴⁷ The initial CE formation enthalpies (denoted as “CE-Initial”) are shown in Figs. 1 and 2 for both W-Ta and W-V alloys. Even at this preliminary stage of fitting the ECIs, the CE technique enables one to make guesses about the ground states of the alloys. For instance, the

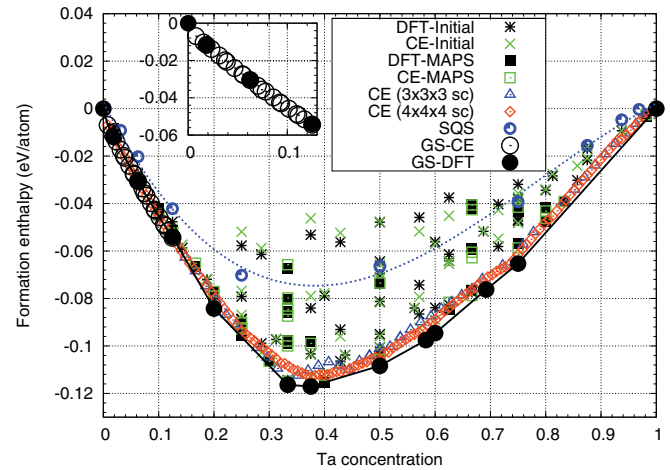


FIG. 1. (Color online) The enthalpy of mixing of W-Ta alloys evaluated using cluster expansion.

$C11_b$ structure is predicted as the lowest energy structure of W_2Ta and W_2V compounds at $T = 0$ K. The initial ECI set serves as a starting point for further automatic refinement of CE parameters, which is achieved by generating new structures, hence enabling the verification of accuracy of predictions made using the ATAT method.³⁹ In this study, the best choice of CE coefficients for both alloys corresponds to the cross-validation error between DFT and CE formation enthalpies (denoted as “DFT-MAPS” and “CE-MAPS,” respectively) of 3.5 meV/atom.

Deriving the final sets of CE parameters, corresponding to the limit where the above criterion is satisfied, involves analyzing more than 100 bcc-like structure types. In order to validate and verify the accuracy of CE parametrization, we use the final ECI sets to calculate the lowest mixing enthalpies of the alloys, which we find using simulated annealing and $3 \times 3 \times 3$ and $4 \times 4 \times 4$ bcc supercells. The relevant data are shown in Figs. 1 and 2 together with the values calculated using the so-called special quasirandom structures (SQS),⁴⁸ which mimic disordered configurations of the alloys.

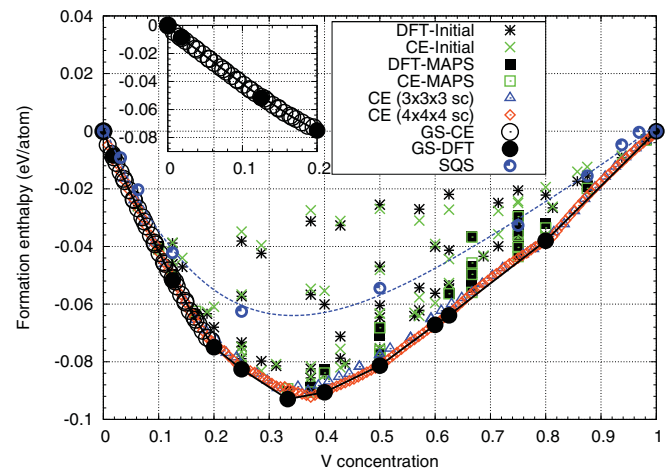


FIG. 2. (Color online) The enthalpy of mixing of W-V alloys evaluated using cluster expansion.

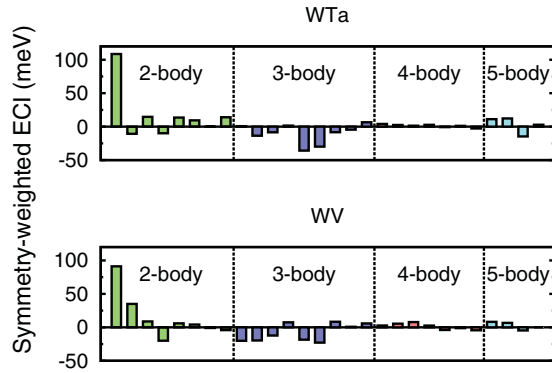


FIG. 3. (Color online) Symmetry-weighted effective cluster interaction parameters for W-Ta and W-V alloys.

The lowest-energy structures predicted using the CE parametrization are shown in Figs. 1 and 2, and are referred to as ground-state CE (GS-CE). Some of those GS-CE stable structures, found using the DFT-Initial and DFT-MAPS sets, are referred to as GS-DFT. For the W-rich part of Figs. 1 and 2, by comparing the enthalpies of formation calculated for stable GS-CE and GS-DFT structures, we find good agreement between the lowest energy atomic configurations predicted by CE and DFT. Insets in Figs. 1 and 2 show how well the enthalpies of mixing calculated using CE and DFT agree in the region from 100 to 80 at. % W.

Figure 3 shows full sets of ECIs for W-Ta and W-V alloys. We have derived eight two-body, nine three-body, seven four-body, and four five-body interaction parameters for both systems. In addition to the fact that our results are in agreement with previous studies^{24,25} in terms of the maximum (five-body) size of the final set of ECIs, we note that the new CE parametrization given here not only includes a more extensive set of pairwise and many-body interactions for W-Ta alloys, but it also represents the first CE parametrization of W-V alloys available in the literature. The values of all the optimized ECIs are given in Appendix A for both W-Ta and W-V alloys. We find that the first nearest-neighbor (1NN) pair interaction is positive and dominant in both cases, implying that the 1NN effective cluster interaction strongly favors *A-B* chemical mixing. The sign of the second-nearest-neighbor (2NN) pair interaction varies; it is negative (-10.704 meV)

for W-Ta and positive ($+34.992$ meV) for W-V. This means that the 2NN atomic environments in W-Ta and W-V alloys are dissimilar. The difference is particularly visible for $x = 1/2$ (i.e., 50% tungsten, 50% Ta or V) alloys. For example, the B_{23} structure, where the 2NN atoms form pairs of *A-A* or *B-B* type, is predicted for the W-Ta alloy, whereas the B_{32} structure, where the 2NN atom pairs are of *A-B* type, is found for the W-V alloy. The prediction of B_{23} structure for the 50 at. % W and 50 at. % Ta alloy agrees with findings by Blum and Zunger.²⁴

Table I shows selected low-energy structures of intermetallic compounds found in CE and DFT calculations. These structures are shown in Figs. 1 and 2 as filled circles. Additional low-energy configurations, shown by open circles in Figs. 1 and 2 in the W-rich region, are found using CE simulations performed using larger unit cells. These low-energy structures are not included in Table III. The ground-state line of the most stable structures was calculated using an algorithm described in Refs. 24 and 25. Information about the space-group symmetry of selected stable structures is given in Appendix B. For W-Ta binary alloys, we found new ordered structures $W_{15}Ta$, W_7Ta , W_4Ta , W_5Ta_3 , W_5Ta_7 , which were not included in the analysis performed earlier.²⁴ In the W-rich region, we found that W_5Ta_3 structure has the lowest enthalpy of mixing (-117.1 meV/atom). This is at variance with previous work^{24,25} where Mo_3Ta_2 (W_3Ta_2) structure appears to have the lowest enthalpy of mixing. Although there is no detailed information about the ECI parameters and enthalpies of mixing in Refs. 24 and 25, the differences can be explained by the fact that we use larger sets of ECIs, which include more many-body interactions, described in Appendix A. The ground-state lowest energy structure curves are also slightly different from those found earlier,^{24,25} for example the enthalpy of mixing for W_2Ta (in $C11_b$ structure) calculated using LDA^{24,25} equals -125 meV/atom, whereas the enthalpy of mixing evaluated for the same structure using GGA is -116 meV/atom.

For W-V binary alloys, none of the predicted low-energy structures ($W_{15}V$, W_7V , W_4V , W_3V , W_2V , W_3V_2 , W_2V_2 , W_2V_3 , W_3V_5 , and W_3V_{12}) were reported previously. The lowest enthalpy of mixing (-92.9 meV/atom) is predicted for the $C11_b$ structure (W_2V), corresponding to an alloy composition containing 66.7 at. % W. The space-group data given in Table III show that although all of the predicted

TABLE I. The lowest energy structures predicted by DFT, CE, and Monte Carlo (MC) simulations for W-Ta and W-V alloys. The enthalpy of mixing ΔH_{mix} is given in eV/atom units, and the order-disorder transition temperatures T_{ord} are given in Kelvin units.

System	Space group	ΔH_{mix}	T_{ord}	System	Space group	ΔH_{mix}	T_{ord}
$W_{15}Ta$	$Pm\bar{3}m$	-0.0275	140	$W_{15}V$	$Pm\bar{3}m$	-0.0258	70
W_7Ta	$Cmmm$	-0.0540	270	W_7V	$I4/mmm$	-0.0518	150
W_4Ta	$I4/mmm$	-0.0843	430	W_4V	$R\bar{3}m$	-0.0750	200
W_2Ta	$I4/mmm$	-0.1164	590	W_3V	$Fm\bar{3}m$	-0.0826	220
W_5Ta_3	$P4/mmm$	-0.1171	600	W_2V	$I4/mmm$	-0.0929	250
W_6Ta_6	$Cmmm$	-0.1084	550	W_3V_2	$R\bar{3}m$	-0.0906	240
W_5Ta_7	$P\bar{3}m1$	-0.0975	500	W_2V_2	$Fd\bar{3}m$	-0.0793	210
W_4Ta_9	$I4/m$	-0.0763	400	W_2V_3	$R\bar{3}m$	-0.0672	180
W_4Ta_{12}	$P4_2/mnm$	-0.0653	330	W_3V_5	$R\bar{3}m$	-0.0629	170
				W_3V_{12}	$R\bar{3}m$	-0.0363	100

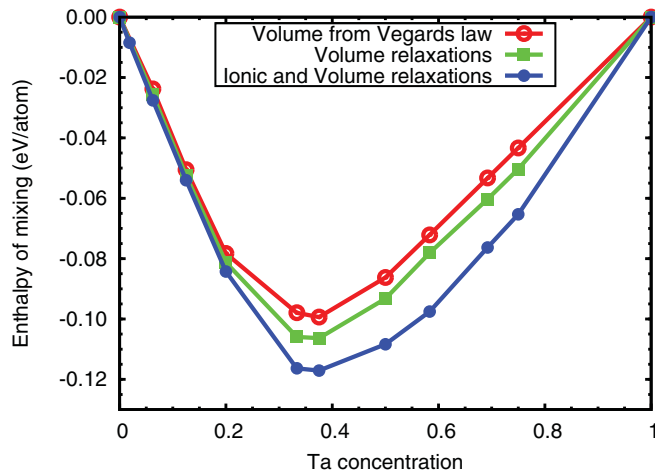


FIG. 4. (Color online) The volume relaxation effect in W-Ta alloys.

intermetallic W-Ta and W-V compounds have crystal structures derived from bcc structure, the majority of them belong to the tetragonal and orthogonal systems, with a relatively small subset of trigonal structures.

Figures 4 and 5 show the effect of volume and atomic relaxations found using DFT for selected low-energy structures for both W-Ta and W-V alloys. In W-Ta alloys (note that Ta is a 5*d* transition metal) relaxations have a more significant impact on the enthalpy of formation of the alloy, especially in the range of relatively high Ta concentration. The W-V alloys are different in this respect, and atomic relaxations in W-V (where vanadium belongs to the 3*d* metal series) do not influence the enthalpy of mixing, despite the fact that the atomic sizes of vanadium and tungsten are quite different. The difference between W-Ta and W-V alloys can probably be explained by the fact that bonding between 3*d*-V and 5*d*-W orbitals has stronger covalent character than covalency characterizing the 5*d*-Ta–5*d*-W bonds. This interpretation is justified in the next section where we compare electronic structures of W-Ta and W-V alloys and investigate chemical SRO characterizing those alloys.

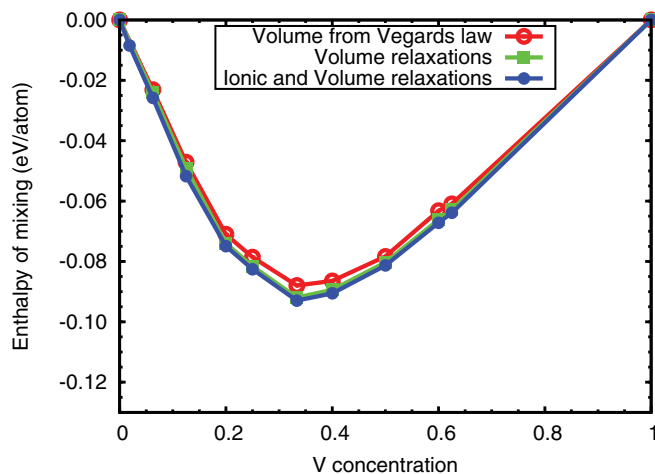


FIG. 5. (Color online) The volume relaxation effect in W-V alloys.

III. ELECTRONIC STRUCTURE AND SHORT-RANGE ORDER

Tungsten has the highest cohesive energy among all the transition metals in the Periodic Table,⁴⁹ and it is not inconceivable that this fact has a bearing on its inter- and trans-granular fracture properties. Its bcc crystal structure and the strength of interatomic bonding are in turn related to the electronic structure of tungsten, and to the fact that it has an approximately half filled 5*d* band with the Fermi energy situated in the pseudominimum of the electronic density of states (DOS).⁵⁰ The pseudominimum separates bonding and antibonding states formed by 5*d* orbitals.

It is appropriate to pose the question of how the electronic structure of W alloys change as a function of the Ta and V content, which in turn is related to the variation of the average number of electrons per atom (*e/a*). The electronic densities of states for several ground-state configurations of W-Ta and W-V alloys are shown in Figs. 6 and 7, respectively. Alloying tungsten with Ta or V, which both have one fewer valence electron than tungsten, alters the behavior of DOS, as shown in Figs. 6 and 7. As the concentration of Ta or V increases, the Fermi energy moves away from the minimum of DOS, and bonding in the alloys becomes less covalent and more metallic. It is important to note here that although all the predicted ground-state structures in W-Ta and W-V alloys have different space-group symmetries in comparison with that of bcc W, Ta, and V, the above analysis of electronic structure as a function of the (*e/a*) ratio shows that it can be well described by the rigid-band approximation. This is also consistent with the fact that all the structures predicted by CE simulations are derived from bcc lattice. We will return to the question about electronic structure in Sec. V, where we apply the Rice-Thompson criterion to assess the ductility of W-Ta and W-V alloys.

Figure 8 shows the finite-temperature enthalpies of mixing of the alloys derived from canonical Monte Carlo simulations performed using a bcc supercell with 20 × 20 × 20 lattice sites. Both curves refer to 50 at.% tungsten alloys, where simulations of W-Ta alloys were performed assuming *T* = 2000 K, whereas the W-V alloys were simulated assuming

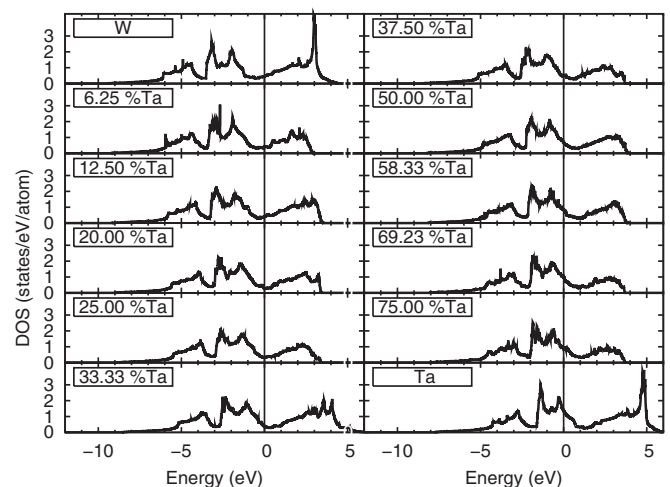


FIG. 6. Electronic density of states calculated for the ground states of W-Ta alloys as a function of Ta content.

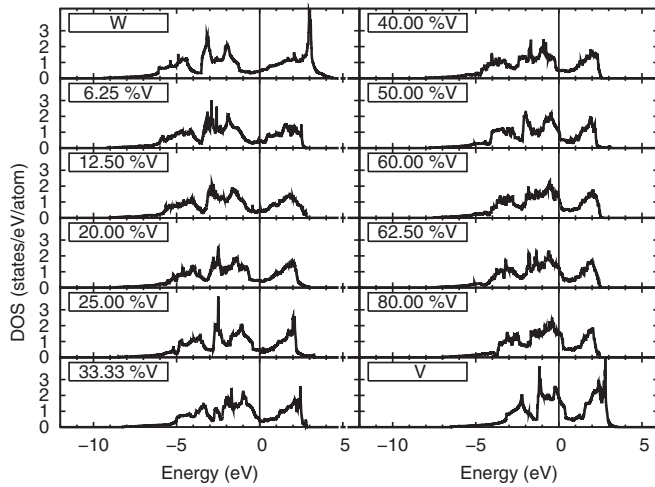


FIG. 7. Electronic density of states calculated for the ground states of W-V alloys as a function of V content.

$T = 1000$ K. We see that the enthalpy of mixing remains negative at high temperatures for both alloys, confirming that the SRO effects and deviations from fully random atomic arrangements play a significant part even in the high-temperature limit. Similar negative enthalpies of mixing at high temperatures were also found in a recent CALPHAD analysis of the W-Ta phase diagram,⁵¹ which involved a somewhat more limited DFT database.²³ There are reasons to believe that these earlier results are less accurate than those described in the present work, as confirmed by the earlier prediction of B_2 and DO_3 structures as ground-state configurations for W-Ta and W_3Ta , respectively. Our results for W-V do not agree with these earlier findings, which were derived from empirical tight-binding simulations, where the latter predict positive enthalpy of mixing for W-V alloys.²⁶ We note that both curves in Fig. 8 show minima at 60 at. % W concentration, which are well correlated with the minima in the enthalpy of formation values found for $T = 0$ K. The order-disorder transition temperatures found using Monte Carlo simulations are given in Table III for several ground-state structures. The maximum ordering temperature is close to 600 K for W-Ta alloys and to 250 K for W-V alloys. These maximum ordering temperature values are well correlated with the minima of the enthalpy of mixing curves predicted by DFT

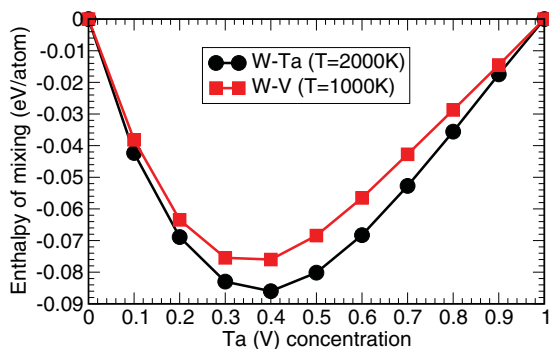


FIG. 8. (Color online) The enthalpy of mixing of W-Ta and W-V alloys at finite temperatures.

calculations. In comparison with previous studies carried out at equiatomic composition ($x = 50\%$), our predicted value of $T_c = 550$ K for W-Ta is higher than the value ($T_c = 360$ K) found in a previous CE investigation.²⁴ The predicted lowest energy crystal structure $B2_3$ is the same in both cases.

Some differences between the present work and those from Ref. 24 can be, however, explained not only by the fact that more ECIs were included in the simulations done here, but also by the fact that we use DFT data sets derived from GGA calculations rather than LDA ones.²⁴ Since the numerical values of the effective cluster interaction parameters used in Ref. 24 were not published, identifying the origin of the differences between the earlier results and our work is difficult. There were four three-body, one four-body, and one five-body interaction parameters included in the earlier study, whereas in the present case the corresponding numbers are 9, 7, and 4, respectively. Hence our work includes many more cluster interactions, and this is probably the main reason why the predicted lowest energy crystal structures are not the same for some compositions. The most notable difference is between the nearest-neighbor effective pair-interaction parameters for W-Ta. We found the value of ≈ 109 meV, whereas the earlier result is ≤ 70 meV; see Ref. 24. In both cases this effective interaction plays the dominant part.

Figure 9 describes order-disorder transitions in both alloys, and illustrates changes in the enthalpy of mixing as well as differences between the transitions themselves. Monte Carlo simulations were performed for three alloy compositions near the minimum of the enthalpy of mixing: W_2Ta , W_5Ta_3 , and W_6Ta_6 in W-Ta and W_2V , W_3V_2 , and W_2V_2 in W-V. The difference between the ordering temperatures found for W_6Ta_6 ($T_c = 550$ K) and W_2V_2 ($T_c = 210$ K) alloys can be explained by the opposite signs of 2NN pair interactions discussed above. We note that the ordering temperature of W_6Ta_6 ($B2_3$) derived from the mixed-basis cluster expansion calculations²⁴ was predicted to be 360 K. A tight-binding-based analysis²⁷ predicts that the transition from the ordered $B2$ structure to the high-temperature disordered bcc phase occurs in WTa at $T = 920$ K. According to our analysis,

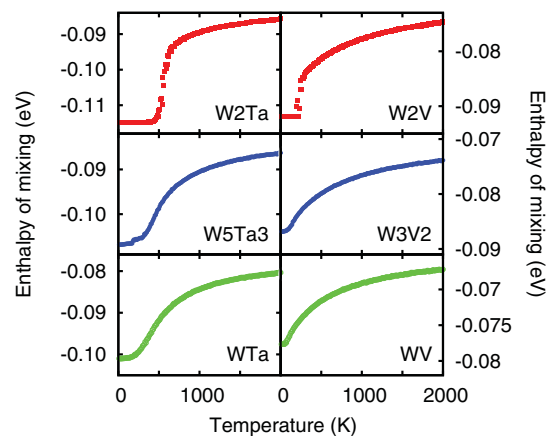


FIG. 9. (Color online) Order to disorder transformations obtained by using Monte Carlo simulations with full set of effective cluster interactions for three ground states W_2Ta , W_5Ta_3 , and W_6Ta_6 and W_2V , W_3V_2 , and W_2V_2 for each binary alloy.

the $B2$ structure has higher enthalpy of mixing than the $B2_3$ structure [$E(B2) - E(B2_3) = 7.8$ meV/atom], and we expect that, as temperature decreases, the alloy first transforms from the high-temperature disordered bcc phase into the $B2$ phase and then from $B2$ to the lowest energy $B2_3$ phase.

The degree of SRO in a binary alloy A_xB_{1-x} can be described using the Warren-Cowley parameters $\alpha_n(x)$, defined as⁵²

$$\alpha_n(x) = 1 - P_n^{B-A}/x, \quad (4)$$

where n is the index of a coordination shell, and P_n^{B-A} is the conditional probability of finding an atom A in the n th coordination shell of atom B . The SRO parameter $\alpha_n(x)$ vanishes if $P_n^{B-A} = x$, meaning that there is no preference for a given atom to be surrounded by atoms of any type. This criterion defines the ideal solid solution limit. Segregation or clustering of atoms of a particular kind give rise to positive $\alpha_n(x)$, whereas negative values of the Warren-Cowley parameter indicate a tendency toward ordering. If in the limit $|1-x| \ll 1$ each atom B is surrounded by A atoms, i.e., $P_n^{B-A} = 1$, then the SRO parameter takes its lowest possible value, $\alpha_n^{\min}(x) = -(1-x)/x$.

The first nearest-neighbor (1NN) and the average between the 1NN and 2NN coordination shells, values of Warren-Cowley parameters derived from equilibrium MC simulations performed on a $10 \times 10 \times 10$ bcc supercell, are shown in Figs. 10 and 11. Simulations were performed for $T = 2000$ K in the case of W-Ta alloys, and for $T = 1000$ K in the case of W-V alloys. The high-temperature results are compared with the corresponding values of SRO parameters calculated for the $T = 0$ K alloy configurations, also derived from MC simulations. For comparison, Figs. 10 and 11 show the function $\alpha_n^{\min} = -x/(1-x)$ for $x < 0.5$, and $\alpha_n^{\min} = -(1-x)/x$ for $x > 0.5$, representing the minimum possible, for a given x , values of the Warren-Cowley parameters for the 1NN coordination shell. We see that the 1NN Warren-Cowley SRO parameters computed from $T = 0$ K CE configurations are negative over the entire range of alloy compositions. For $x \leq 0.3$ and $x \geq 0.70$, complete ordering is found for both binary systems, confirmed by the fact that the calculated

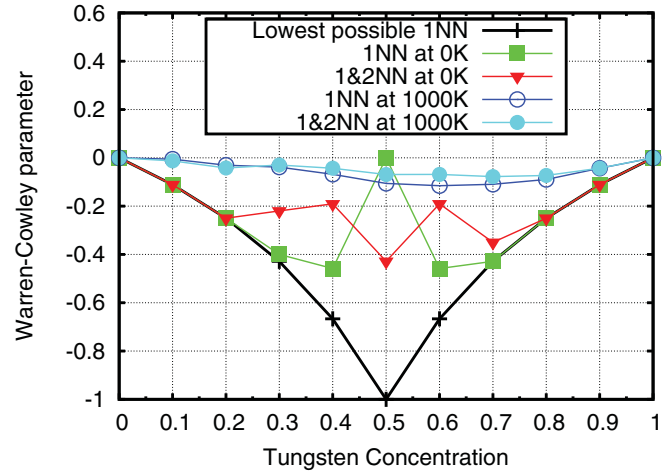


FIG. 11. (Color online) The Warren-Cowley short-range order parameters evaluated for W-V alloys.

values of the 1NN SRO parameters approach the minimum possible values. In the 30–70 at. % W composition range, the Warren-Cowley parameters computed for the 1NN shell shows a lesser degree of ordering. In particular, the zero value of the 1NN Warren-Cowley parameter for the 50 at. % W alloy comes from the atomic environment of the $B32$ lowest energy structure. The average, between the 1NN and 2NN shells, SRO parameters found for $T = 0$ K show partial ordering between 20 and 80 at. % W for both alloys. At high temperatures ($T = 2000$ K for W-Ta and $T = 1000$ K for W-V), where alloys adopt disordered solid solution bcc configurations, the values of SRO parameters evaluated from full CE simulations are negative but small. This confirms that deviations from the solid solution behavior seen in both alloys at high temperature is due to the presence of SRO, in agreement with experimental observations.²²

IV. POINT DEFECT PROPERTIES

We start from the investigation of formation energies of self-interstitial atom (SIA) and monovacancy defects in pure bcc tungsten and dilute tungsten alloys. The calculations are carried out using $4 \times 4 \times 4$ bcc supercells containing 128 atoms and a $3 \times 3 \times 3$ mesh of k points.

TABLE II. Formation energies (in eV) of self-interstitial atom and vacancy defects in tungsten and dilute tungsten alloys.

Defect configuration	Defect composition				
	W-W	W-Ta	W-V	Ta-Ta	V-V
$\langle 111 \rangle$	10.086	10.251	7.810	10.533	5.993
$\langle 110 \rangle$	10.545	10.858	8.320	11.218	5.636
$\langle 100 \rangle$	12.200	12.349	9.582	12.703	7.348
Vacancy-1NN		3.378	3.265		
Vacancy-2NN		3.544	3.266		
Vacancy-3NN		3.445	3.131		
Vacancy-4NN		3.366	3.089		
Vacancy-5NN		3.397	3.123		
Vacancy-6NN		3.330	3.081		

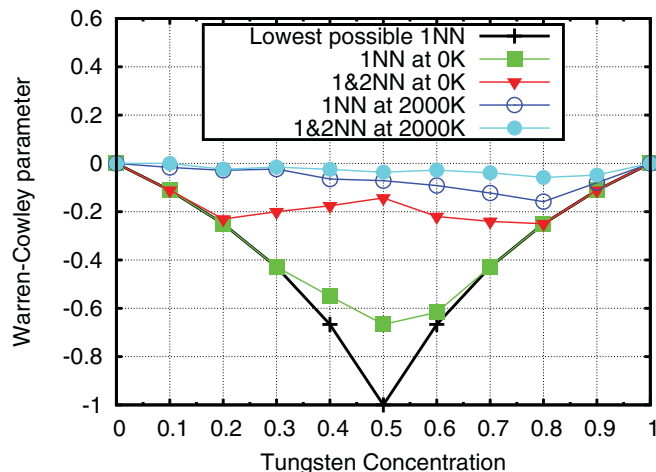


FIG. 10. (Color online) The Warren-Cowley short-range order parameters evaluated for W-Ta alloys.

The calculated formation energies are given in Table II where the reference energies per atom for pure bcc tungsten, tantalum, and vanadium were calculated using the same $4 \times 4 \times 4$ bcc supercells. In agreement with previous studies,^{28,30} we found that the $\langle 111 \rangle$ SIA configuration has the lowest formation energy. We note that although the SIA formation energy has been recently measured using low-temperature evaporation of tungsten in a field-ion microscope, observations gave no information about the structure of single SIA configurations.⁵³ $\langle 111 \rangle$ crowdion cluster configurations were observed using *in situ* electron transmission microscopy in bcc iron⁵⁴ and tungsten.⁵⁵

The $\langle 110 \rangle$ and $\langle 100 \rangle$ dumbbell configurations both have higher formation energies than that of a $\langle 111 \rangle$ crowdion. To investigate how this relation changes in an alloy, we calculated formation energies of mixed W-Ta and W-V dumbbells, as well as of Ta-Ta and V-V dumbbells, assuming pure tungsten environment. The data given in Table II show that, with the exception of the V-V SIA defect, the $\langle 111 \rangle$ dumbbell configuration remains the most stable in all cases but one. We find that the V-V SIA dumbbell adopts the $\langle 110 \rangle$ configuration with the formation energy of 5.636 eV. The fact that the $\langle 110 \rangle$ SIA configuration has the lowest formation energy for a Re-Re dumbbell (again, assuming the matrix of pure W) was recently reported in Ref. 56. We note that, similarly to a rhenium atom, a vanadium atom has smaller size than a tungsten atom, whereas a Ta atom has the size greater than that of a tungsten atom. The formation energies of a vacancy interacting with an impurity Ta (or V) atom, which is situated 1NN, 2NN, ..., 6NN distance away from the vacancy, are also given in Table II. The vacancy formation energy decreases smoothly as the distance between the vacancy and an impurity atom decreases from the 1NN to 4NN distance, then it slightly increases at the 5NN interatomic separation, before decreasing again at the 6NN separation.

Before moving on to the investigation of vacancies in W-Ta and W-V alloys, we evaluate the energies of formation of small vacancy clusters in bcc-W, which are important for modeling kinetics of nucleation and growth of voids in tungsten under irradiation.^{57–59} Table III shows the calculated formation and binding energies of small clusters of vacancies ($N_v = 2–6$) calculated for pure tungsten using the PBE-GGA

TABLE III. Formation energies (E_f) and binding energies (E_b), in eV, of vacancy clusters in tungsten. Positive values of the binding energy indicate attraction between the vacancies, leading to clustering of vacancies, whereas negative values indicate repulsion.

Cluster	PBE E_f	PBE-AM05 E_f	PBE E_b	PBE-AM05 E_b
1	3.327	3.568		
2 ($\langle 111 \rangle$)	6.624	7.129	0.029	0.007
2 ($\langle 100 \rangle$)	6.989	7.325	−0.365	−0.190
3	9.711	10.454	0.269	0.250
4	12.242	13.398	1.065	0.874
5	14.669	16.103	1.965	1.736
5 (Ref. 71)	15.744	17.230	0.890	0.610
6	17.847	19.457	2.113	1.950

exchange-correlation functional⁴³ with semicore electrons included in the PAW potential implemented within the VASP code. The calculated formation energies for the first-nearest-neighbor and second-nearest-neighbor divacancies are 6.624 and 6.989 eV, respectively, in agreement with values found previously (6.71 and 6.93 eV) using the PLATO code and atomiclike orbital basis sets.^{28,30} The monovacancy formation energy of 3.327 eV found in the present work is 0.23 eV lower than the value 3.56 eV found earlier using the PLATO code.^{28,30} We note that the earlier VASP calculations^{60–62} carried out using a different exchange-correlation functional⁶³ and a smaller energy cutoff of 240 eV, as opposed to 400 eV used here, predicted an even lower vacancy formation energy of 3.11 eV. *Ab initio* investigation of defects in tungsten carried out using SIESTA code⁶⁴ found vacancy formation energies in the range between 3.2 and 3.3 eV, in agreement with the values given in Table V.

To estimate the contribution to the vacancy formation energy from exchange-correlation effects we investigated how this energy depends on the choice of exchange-correlation functional. By using the AM05 functional,⁶⁵ which provides a reasonably accurate treatment of systems with open surfaces, for example vacancies or vacancy clusters, we found the formation energy for a monovacancy in bcc W of 3.57 eV. The latter value correlates well with the earlier values found using the PLATO code^{28,30} and it also agrees with experimental data for bcc-W showing that the vacancy formation energy lies in the interval between 3.5 and 4.1 eV.²⁸ The fact that the monovacancy formation energy appears to be sensitive to the choice of exchange-correlation functional and that it varies in a relatively broad interval between 3.11 eV^{60–62} and 3.56 eV^{28,30} warrants further analysis.

The calculated binding energies of vacancy clusters shown in Fig. 12 are all positive, apart from the 2NN divacancy configuration. The binding energy for a divacancy cluster $E_{2v}^b = 2E_v^f - E_{2v}^f$, where E_v^f and E_{2v}^f are the formation energies for a monovacancy and a divacancy, in the 1NN divacancy configuration is fairly small (0.029 eV), whereas the binding energy for a divacancy in the 2NN configuration is negative (−0.365 eV) and the two vacancies repel each other. These results, found using the VASP code, are broadly consistent with binding energies of 0.05 and −0.27 eV for the 1NN and 2NN divacancy configurations reported recently in Ref. 66 whereas earlier experimental work performed using field ion microscopy and showing vacancy clusters formed at free surface indicate that the favorable configurations of divacancies in tungsten are of the 1NN type.⁶⁷

There is another reason why one should expect unusual properties of divacancies in tungsten. The strength of elastic interaction between two vacancies in a cubic crystal depends on the degree of elastic anisotropy of the material.^{68,69} Tungsten is elastically isotropic, i.e., in tungsten the difference $C_{11} - C_{12} - 2C_{44}$ is very close to zero, resulting in that the self-energy of a line dislocation is independent of the orientation of the dislocation line with respect to the lattice,⁷⁰ and in that the strength of *elastic* interaction between two vacancies is anomalously small in comparison with other bcc metals; see Eq. (13) of Ref. 69.

The binding energy of a vacancy cluster in the $N_v = 3-6$ range increases with the number of vacancies in a cluster, as shown in Table III. We find that the lowest energy configuration for a cluster of five vacancies is different from the square pyramid shape found in simulations performed using empirical potentials.⁷¹ For the latter configuration, the formation and binding energies found in DFT calculations are also shown in the table. The formation energy of the square pyramid configuration is 1.075 eV higher than the formation energy of the five-vacancy cluster shown in Fig. 12. Positron annihilation measurements suggest that vacancies form clusters at ≈ 650 K and that the size of clusters varies in the range $N_v = 4-10$.⁵⁷ Table III also shows the formation and binding energies for vacancy clusters computed using another exchange-correlation energy functional, AM05.⁶⁵ We find trends similar to those found using the PBE functional.

We now investigate monovacancy formation energies for a selected set of ground-state structures of W-Ta and W-V alloys. For example, the formation energy of a vacancy removed from a crystallographic site occupied by a W atom is defined as

$$E_{\text{vacancy in } X\text{-W, } Y\text{-Ta(V)}}^f = E^{(X-1)\text{-W, } Y\text{-Ta(V)}} - E^{X\text{-W, } Y\text{-Ta(V)}} + \frac{1}{128} E^{128\text{W}}, \quad (5)$$

where X and Y denote the number of tungsten and tantalum (or vanadium) atoms in the 128-atom unit cell of compound W_XTa_Y . $E^{(X-1)\text{-W, } Y\text{-Ta(V)}}$ is the energy of a configuration with a vacancy on a tungsten site, $E^{X\text{-W, } Y\text{-Ta(V)}}$ is the energy of the alloy with no defect, and $E^{128\text{W}}$ is the energy of a bcc cell

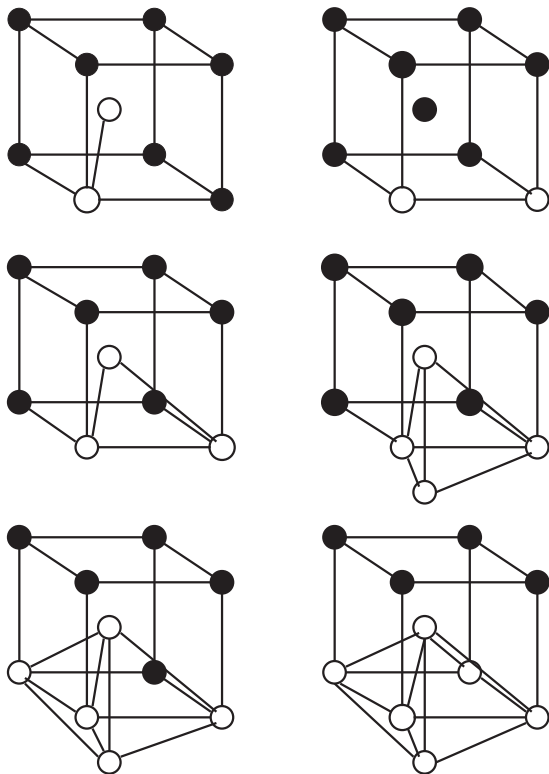


FIG. 12. Tungsten vacancy cluster configurations ($N_v = 2-6$) investigated in the present study.

containing 128 tungsten atoms. Here we use pure bcc W (or Ta, V) as a reference for calculating vacancy formation energies. A more accurate determination of W (or Ta, V) chemical potential referring to a particular constituting element in an intermetallic compound involves taking into account not only vacancies at each lattice site of the structure (see Appendix B) but also other possible point defects such as antisite defects or self-interstitials.

Figure 13 shows formation energies of monovacancy defects, calculated for a number of lattice sites characterized by the space groups given in Table I. The formation energy for a monovacancy in W-Ta strongly depends on the environment of a vacancy site, varying by as much as 2 eV between Ta and W sites. The origin of the effect is likely associated with atomic volume mismatch between the tungsten and tantalum atoms. The case of W-V alloys is very different in that we do not find any significant variation between the formation energies of vanadium or tungsten vacancies. Tables IV and V summarize the calculated values of vacancy formation energies shown in Fig. 13 for W-Ta and W-V binaries. The Wyckoff positions denote the crystallographic symmetry of each site occupied by W, Ta, or V atoms.

Finally, we investigate the strength of interaction between a $\langle 111 \rangle$ SIA crowdion with Ta and V impurity atoms. We define the binding energy of this interaction, say between a crowdion and a Ta atom, as

$$E_{\text{crowdion}}^b = E_{\text{crowdion}}^{129\text{W}} + E^{127\text{W}1\text{Ta}} - E^{128\text{W}} - E_{\text{crowdion}}^{128\text{W}1\text{Ta}}, \quad (6)$$

where $E_{\text{crowdion}}^{129\text{W}}$ is the energy of a crowdion in pure tungsten, $E^{127\text{W}1\text{Ta}}$ is the energy of a defect-free 127W1Ta alloy system, $E^{128\text{W}}$ is the energy of an ideal bcc W cell containing 128 atoms, and $E_{\text{crowdion}}^{128\text{W}1\text{Ta}}$ is the energy of a crowdion in 128W1Ta alloy.

Figure 14 shows how the binding energy of interaction between a crowdion and a V or a Ta or a Re atom in bcc tungsten varies as a function of the position of an impurity atom in a $\langle 111 \rangle$ string containing the crowdion defect. We find that the binding energy is positive (attraction) for a vanadium

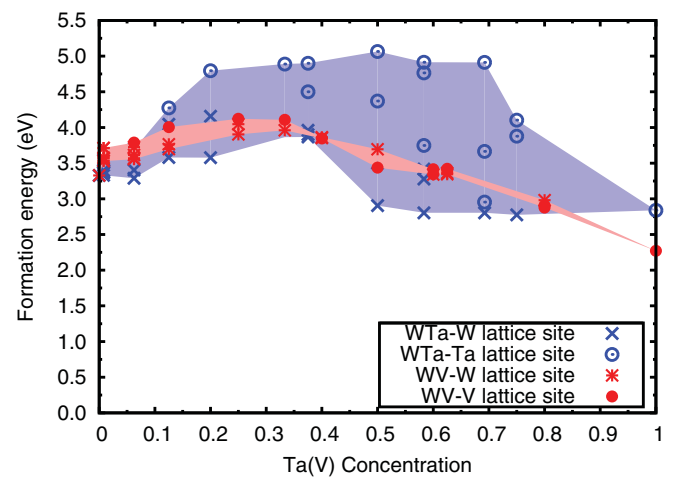


FIG. 13. (Color online) Monovacancy formation energies computed for the ground-state intermetallic structures of W-Ta and W-V binary alloys.

TABLE IV. Vacancy formation energy computed for the ground states of W-Ta alloys. The formation energy equals $E_f^v = E_V^{\text{tot}}(N-1) - E^{\text{tot}} + E^X$, where E_V^{tot} and E^{tot} are the total energies of alloys with and without a vacancy. E^X is the energy of an atom in a W or Ta crystal, depending on the lattice site where the vacancy was created.

Ground-state	Lattice site	Wyckoff position	E_f^v (eV)	Ground-state	Lattice site	Wyckoff position	E_f^v (eV)
W ₁₅ Ta	W	1b	3.289	W ₆ Ta ₆	W	2d	2.905
	W	3c	3.403		W	4g	3.498
	W	3d	3.692		Ta	2b	5.066
	W	8g	3.695		Ta	4h	4.371
	Ta	1a	3.652		W ₅ Ta ₇	W	1a
W ₇ Ta	W	2d	3.580	W		2d	2.804
	W	4f	4.045	W		2d	3.417
	W	4g	3.673	Ta		2c	4.765
	W	4i	3.985	Ta		2d	4.748
	Ta	2a	4.275	Ta	2d	4.915	
W ₄ Ta	W	4e	3.577	W ₄ Ta ₉	Ta	2d	4.850
	W	4e	4.157		W	8h	2.804
	Ta	2b	4.796		Ta	2a	2.954
W ₂ Ta	W	4e	3.865	W ₄ Ta ₁₂	Ta	8h	3.665
	Ta	2a	4.890		Ta	8h	4.912
W ₅ Ta ₃	W	1a	3.867	W ₄ Ta ₁₂	W	4f	2.775
	W	2g	3.900		Ta	4f	3.878
	W	2h	3.960		Ta	8i	4.103
	Ta	1b	4.502				
	Ta	2h	4.896				

atom, and that the binding energy is negative (repulsion) for a tantalum atom. For comparison, Fig. 14 also shows the binding energy of interaction between a crowdion and a rhenium atom. We see that the cases of V and Re are similar, and in this case the binding energy of interaction between a defect and an impurity atom is positive (i.e., the defect and an impurity atom form a bound configuration). Figure 14 suggests that V and Re substitutional impurities trap SIA defects in bcc-W, and this

should be expected to affect microstructural evolution of the alloys under irradiation; see, for example, Refs. 72 and 73. The pattern of interaction between a SIA defect in tungsten and V or Re atoms is somewhat similar to that found by Olsson *et al.*⁷⁴ for the case of a $\langle 111 \rangle$ crowdion defect in bcc *iron* interacting with manganese and chromium impurity atoms. Comparing the effect of Re and V impurities, we find that vanadium atoms trap SIA defects stronger than rhenium atoms.

TABLE V. Vacancy formation energy computed for the ground states of W-V alloys. The formation energy equals $E_f^v = E_V^{\text{tot}}(N-1) - E^{\text{tot}} + E^X$, where E_V^{tot} and E^{tot} are the total energies of alloys with and without a vacancy. E^X is the energy of an atom in a W or V crystal, depending on the lattice site where the vacancy was created.

Ground-state	Lattice site	Wyckoff position	E_f^v (eV)	Ground-state	Lattice site	Wyckoff position	E_f^v (eV)	
W ₁₅ V	W	1b	3.555	W ₃ V ₂	W	3a	3.864	
	W	3c	3.568		W	6c	3.852	
	W	3d	3.614		V	6c	3.847	
	W ₇ V	W	8g	3.724	W ₂ V ₂	W	8a	3.695
		W	1a	3.788		V	8b	3.437
W		2b	3.697	W ₂ V ₃	W	6c	3.341	
W ₄ V	W	4e	3.705		V	3b	3.345	
	W	8g	3.764		V	6c	3.416	
	V	2a	4.005	W ₃ V ₅	W	3a	3.345	
W ₃ V	W	6c	3.704		W	6c	3.364	
	W	6c	3.755		V	3b	3.421	
	V	3b	3.988	V	6c	3.402		
W ₂ V	W	4b	3.903	W ₃ V ₁₂	V	6c	3.412	
	W	8c	4.046		W	3a	2.980	
	V	4a	4.122		V	6c	2.878	
W ₂ V	W	4e	4.107		V	6c	2.909	
	V	2a	3.960					

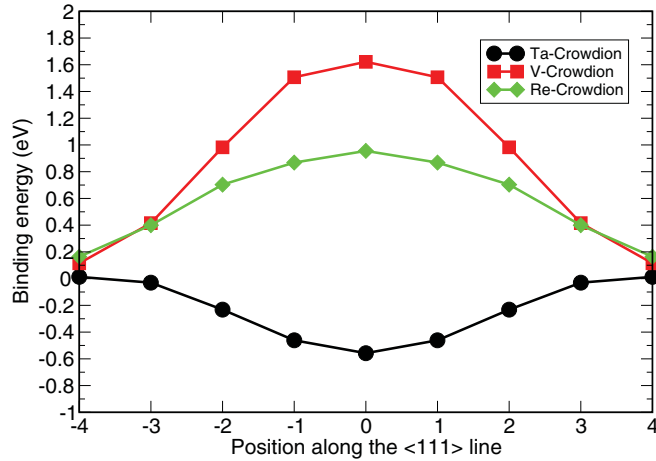


FIG. 14. (Color online) Binding energy of a crowdion interacting with substitutional Ta, V, and Re atoms in bcc-W lattice.

V. ELASTIC CONSTANTS OF W-V AND W-TA ALLOYS

Elastic properties of W-Ta and W-V alloys were investigated using fully relaxed and optimized lowest energy structures derived from DFT total-energy calculations. Using a single distortion for each of the necessary strains, it is possible to find all the elastic constants for a given atomic structure. Several strains can be used to provide more data points for the fitting procedure, thus leading to higher accuracy and better numerical stability of the method. A large number of k points was used in these calculations, with the spacing between the k points approaching 0.01 \AA^{-1} . Table VI summarizes values of elastic constants calculated for all the ground-state structures predicted for W-Ta and W-V binaries, which mostly

form structures with lower symmetry than cubic. Only the independent elastic constants for a given crystallographic symmetry of the underlying crystal structure are shown in the table. All the eigenvalues of the elastic constant matrices are positive, confirming that the compounds are mechanically stable at low temperature. Experimentally measured values of elastic constants found assuming cubic symmetry of the lattice are available for W-Ta alloys for various Ta compositions.⁷⁵ Our DFT analysis shows that the only cubic lowest energy W-Ta alloy structure is $W_{15}Ta$, for which the calculated values of elastic constants are $C_{11} = 497 \text{ GPa}$, $C_{12} = 197 \text{ GPa}$, and $C_{44} = 134 \text{ GPa}$. Comparing them with the corresponding experimental values of $C_{11} = 482 \text{ GPa}$, $C_{12} = 196 \text{ GPa}$, and $C_{44} = 139 \text{ GPa}$ determined at $T = 4.2 \text{ K}$ for a W-rich alloy composition ($x = 83\%$), we find good agreement between theory and experiment. Comparison with elastic constants found for pure bcc-W shows that all the elastic constants for $W_{15}Ta$ are lower, in agreement with experimental observations.

More detailed analysis of elastic constants data shown in Table VI will be given elsewhere. Here we focus on the anisotropic elastic properties of several cubic structures, which are the closest metastable matches to the configurations found as ground states. For a single crystal, the Young modulus in a particular crystallographic direction is defined as follows. If tensile stress is applied in a particular direction, the ratio of stress to strain in the same direction equals the Young modulus. In a cubic crystal, the reciprocal of the Young modulus is given by the following equation:³²

$$E^{-1} = s_{11} - 2[s_{11} - s_{12} - (1/2)s_{44}][(\alpha_{11})^2(\alpha_{12})^2 + (\alpha_{11})^2(\alpha_{13})^2 + (\alpha_{12})^2(\alpha_{13})^2], \quad (7)$$

where α_{11} , α_{12} , and α_{13} are the cosines of the angles between a chosen direction ($[100]$ in the present study) and the three

TABLE VI. Results of first-principles calculations of various independent elastic constants (in GPa) found for W-Ta and W-V ground-state structures of the alloys.

System	C_{11}	C_{12}	C_{13}	C_{15}	C_{23}	C_{24}	C_{25}	C_{33}	C_{44}	C_{46}	C_{55}
$W_{15}Ta$	497	197							134		
W_7Ta	497	183		1.3	185		-1.7	495	126	1.8	139
W_4Ta	484	183	188					472	124		125
W_2Ta	452	169	179					471	112		124
W_5Ta_3	424	189	178					417	96		97
W_6Ta_6	369	184		5.7	185		-6.9	370	66	-13.4	73
W_5Ta_7	352	179		4.5			-3.2		75	-9.1	
W_4Ta_9	396	214	206			0.4		406	97		83
W_4Ta_{12}	352	150			159			341	88		80
$W_{15}V$	495	195							132		
W_7V	467	234			189			512	160		123
W_4V	451	191		13	201			441	130		137
W_3V	464	184							101		
W_2V	454	166	174					455	95		99
W_3V_2	400	192		29	214			395	104		117
W_2V_2	359	184							49		
W_2V_3	276	183		21	193			290	47		61
W_3V_5	281	173		19	181			303	54		69
W_3V_{12}	233	144		17	146			250	45		62

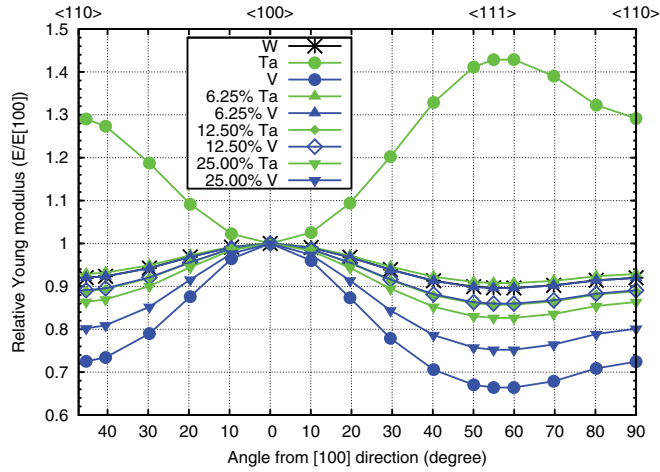


FIG. 15. (Color online) Angular dependence of the relative Young modulus of W-Ta and W-V alloys.

Cartesian axes. The compliances s_{ij} are expressed in terms of the stiffness (or elastic) constants C_{ij} . Equation (7) is used for investigating the anisotropy behavior of the calculated Young moduli for W-Ta and W-V alloys. For polycrystalline samples, we use the Voigt-Reuss-Hill method to evaluate the effective shear modulus G as

$$G_{\text{Hill}} = (1/2)(G_{\text{Voigt}} + G_{\text{Reuss}}), \quad (8)$$

where $G_{\text{Voigt}} = (1/5)(C_{11} - C_{12} + 3C_{44})$ and $G_{\text{Reuss}} = 5/[4(s_{11} - s_{12}) + 3s_{44}]$. The Poisson ratio ν is given by a theory of elasticity formula relating it to the shear (G) and the bulk (B) moduli via

$$\nu = \frac{B - (2/3)G}{2[B + (1/3)G]}. \quad (9)$$

Figure 15 shows variation of the anisotropic Young modulus, evaluated using Eq. (7) for pure bcc W, Ta, and V, and several alloys, using the values of elastic constants found in DFT calculations. The results for pure metals are in agreement with experimental observations. For pure tungsten the Young

modulus is almost isotropic, i.e., it is independent of the crystallographic direction in which the material is deformed, whereas in pure tantalum the modulus has a strong maximum in the [111] direction. In pure vanadium the maximum is in the [100] direction. The W-rich Ta and V alloys (containing 6.25%, 12.5%, and 25% of alloying elements) appear more anisotropic than pure bcc-W. The Young modulus is maximum in the [100] direction. These predictions can be verified using the recently developed technique for measuring the anisotropy of Young's modulus by means of microcantilever testing.⁷⁶

Table VII shows the DFT predicted change in the Poisson ratio [Eq. (9)] for the three alloys (containing 6.25%, 12.5%, and 25% of Ta or V) and compares the results with those found for bcc-W. Our calculations show that alloying increases the Poisson ratio in comparison with pure tungsten. In particular, we find that the addition of 6.25% V (or Ta) increases the Poisson ratio by less than 2.5% whereas for 25% V or Ta alloys we find a 9.7% or 7.11% increase of the Poisson ratio, respectively. According to Cottrell's criterion,⁷⁷ the value of the Poisson ratio is correlated with the ductility of crystalline alloys, namely the higher the Poisson ratio, the more ductile is the metal.

In Table VII we also show values of the Rice-Thompson parameter ($b\mu/\gamma$),⁷⁸ using which one could assess the effect of alloying on the ductility of the material. Here \mathbf{b} and μ denote the Burgers vector of a dislocation and the shear modulus, respectively, in the preferred slip plane. γ is the surface energy corresponding to the fracture plane. In the present study we consider the (110) slip plane. Applying the Rice-Thompson criterion, we take that materials where the ratio ($b\mu/\gamma$) exceeds 10 tend to be brittle and those where the ratio ($b\mu/\gamma$) ≤ 10 tend to deform in a ductile manner. Our DFT calculations show that for W alloys with 25% of V or Ta, this ratio decreases by about 32% from the value characterizing pure W, changing from ($b\mu/\gamma$) = 13.834 for pure W to 9.288 or 9.375 for the 25% V or Ta alloys, respectively. It is important to stress here that better understanding of brittle fracture requires applying a microscopic criterion where plastic work is a nonlinear function of γ , the ideal work for fracture, which in turn depends strongly on the cohesive energy of

TABLE VII. The calculated values of the Pugh-Cottrell (PC) and Rice-Thompson (RT) criteria for ductilizing W by Ta and V alloying.

	W	W ₁₅ Ta	W ₁₅ V	W ₇ Ta	W ₇ V	W ₃ Ta	W ₃ V
Space group	$Im\bar{3}m$	$Pm\bar{3}m$	$Pm\bar{3}m$	$Pm\bar{3}m$	$Pm\bar{3}m$	$Fm\bar{3}m$	$Fm\bar{3}m$
C_{11} (GPa)	526	497	495	506	501	459	464
C_{12} (GPa)	194	197	195	190	186	185	184
C_{44} (GPa)	146	134	132	132	132	110	101
B (GPa)	314	297	295	295	291	276	277
G_{Voigt} (GPa)	154	140	139	156	142	121	117
G_{Reuss} (GPa)	153	140	139	154	141	119	114
G_{Hill} (GPa)	154	140	139	155	142	120	115
ν	0.289	0.296	0.296	0.293	0.291	0.310	0.318
Change in ν (%)	0.0	2.28	2.31	1.17	0.35	7.11	9.70
μ (GPa)	166	150	150	158	158	137	140
b (Å)	2.771	2.770	2.753	2.773	2.743	2.788	2.720
γ (J/m ²)	3.325	3.197	3.147	3.234	3.243	4.074	4.100
$b\mu/\gamma$	13.834	12.997	13.122	13.548	13.364	9.375	9.288
Change in $b\mu/\gamma$ (%)	0.0	-6.05	-5.15	-2.07	-3.40	-32.23	-32.86

the materials.⁴⁹ Performing this analysis would require going beyond the scope of the present DFT study.

VI. CONCLUSIONS

In this work, we investigated the phase stability of W-Ta and W-V alloys by combining DFT, cluster expansion and Monte Carlo simulations, and explored the relatively low-temperature part of the phase diagram of these alloys. Both alloys are characterized by negative enthalpies of mixing, and a significant degree of chemical SRO. The results show that both W-Ta and W-V alloys are characterized by significant deviations from the random solution limit, at variance with conventional understanding of experimental high-temperature phase diagrams. We find differences between SRO parameters characterizing W-Ta and W-V alloys, which stem mainly from the fact that the 2NN effective CE interaction parameter changes sign in W-Ta in comparison with W-V: it is negative for W-Ta but positive in W-V. The origin of this difference is related to the difference between $5d-3d$ and $5d-5d$ metallic bonding in the two alloys. This interpretation is confirmed by the effect of volume and atomic relaxation on the enthalpy of mixing across the entire range of composition of the alloys.

Using DFT, we have also investigated the structure and stability of point defects formed in the alloys under irradiation. DFT calculations, carried out using the PBE exchange-correlation functional, showed that divacancy binding in tungsten is weak, but the stability of a vacancy cluster increases as a function of the number of vacancies in the cluster. By exploring various SIA configurations and their interaction with alloying elements, we found that a stable $\langle 110 \rangle$ dumbbell SIA configuration may form in W-V alloys near V-V atom pairs whereas the $\langle 111 \rangle$ SIA configuration represents the most stable defect structure even in the presence of V and Ta impurities, and even the pairs of Ta atoms. We have also explored the vacancy formation energy in both alloys as a function of Ta and V concentration. Our results show that the atomic size mismatch has a profound effect on monovacancy formation energies. For example, the removal of a Ta atom from an W-Ta ordered intermetallic compound results in the vacancy formation energy that is different by more than 2 eV from the energy associated with forming a vacancy at a W site. On the other hand, this difference is almost negligible in the case of W-V alloys. We also find that the energy of binding between a crowdion and a vanadium impurity atom in W-V alloy is positive, and V atoms are expected to trap SIA defects in dilute W-V alloys. Finally, we have created a database of low-temperature elastic constants for both W-Ta and W-V binary alloys, which shows a significant degree of elastic anisotropy characterizing the alloys. Applying DFT to the evaluation of the Rice-Thompson parameter, we find that alloying tungsten with more than 25% of V or Ta would reduce the ratio $(b\mu/\gamma)$ by more than 30% in comparison with pure W, possibly resulting in the improved ductility of the materials.

ACKNOWLEDGMENTS

This work, partially funded by the European Communities under the contract of Association between EURATOM and Polish, CCFE, and Swiss Associations, was carried out

within the framework of the European Fusion Development Agreement. This work was also partially funded by the RCUK Energy Programme under Grant No. EP/1501045. The authors would like to thank D. E. J. Armstrong, C. S. Becquart, M. R. Gilbert, C.-C. Fu, K. Heinola, M. Reith, S. G. Roberts, V. Vitek, and F. Willaime for stimulating discussions. M.M. acknowledges support from EURATOM staff mobility program, and hospitality at Culham Centre for Fusion Energy, where most of the results described in the present study were produced. D.N.M. would like to acknowledge the use of High Performance Computing for Fusion facilities at Julich.

APPENDIX A: EFFECTIVE CLUSTER INTERACTIONS FOR W-Ta AND W-V ALLOYS

Tables VIII and IX contain complete sets of values of effective cluster interaction coefficients for W-Ta and W-V binary systems.

APPENDIX B: RELAXED LOW-ENERGY STRUCTURES OF W-Ta AND W-V BINARY ALLOYS

W₁₅Ta

Space group: $Pm\bar{3}m$ (no. 221).

Lattice constant:

$$a = 6.39130 \text{ \AA}$$

Wyckoff positions:

$$W_1 1b(\frac{1}{2}, \frac{1}{2}, \frac{1}{2})$$

$$W_2 3c(0, \frac{1}{2}, \frac{1}{2})$$

$$W_3 3d(\frac{1}{2}, 0, 0)$$

$$W_4 8g(0.25104, 0.25104, 0.25104)$$

$$Ta_1 1a(0, 0, 0)$$

W₇Ta

Space group: $Cmmm$ (no. 65).

Lattice constants:

$$a = 6.40825 \text{ \AA}, b = 9.04500 \text{ \AA}, c = 4.52942 \text{ \AA}$$

Wyckoff positions:

$$W_1 2d(0, 0, \frac{1}{2})$$

$$W_2 4f(\frac{1}{4}, \frac{1}{4}, \frac{1}{2})$$

$$W_3 4g(0.24792, 0, 0)$$

$$W_4 4i(0, 0.25036, 0)$$

$$Ta_1 2a(0, 0, 0)$$

W₄Ta

Space group: $I4/mmm$ (no. 139).

Lattice constants:

$$a = 3.15157 \text{ \AA}, c = 15.72395 \text{ \AA}$$

Wyckoff positions:

$$W_1 4e(0, 0, 0.09727)$$

$$W_2 4e(0, 0, 0.30158)$$

$$Ta_1 2b(0, 0, \frac{1}{2})$$

W₂Ta

Space group: $I4/mmm$ (no. 139).

Lattice constants:

$$a = 3.22105 \text{ \AA}, c = 9.70284 \text{ \AA}$$

Wyckoff positions:

$$W_1 4e(0, 0, 0.32977)$$

$$Ta_1 2a(0, 0, 0)$$

W₅Ta₃

Space group: $P4/mmm$ (no. 123).

Lattice constants:

TABLE VIII. Many-body effective cluster interactions (in meV) derived for W-Ta binary alloys

No. of points	m_α	Points in clusters	Symmetry-weighted ECI
0	1		-150.435
1	2	(0.0,0.0,0.0)	84.152
2	8	(0.0,0.0,0.0;0.5,0.5,0.5)	108.568
2	6	(0.0,0.0,0.0;1.0,0.0,0.0)	-10.704
2	12	(0.0,0.0,0.0;1.0,0.0,-1.0)	14.592
2	24	(0.0,0.0,0.0;0.0,1.5,0.0)	-9.840
2	8	(0.5,0.5,0.5;1.5,1.5,-0.5)	13.568
2	6	(0.0,0.0,0.0;0.0,0.0,2.0)	9.348
2	24	(0.0,0.0,0.0;1.5,1.5,0.5)	-0.168
2	24	(0.0,0.0,0.0;-2,1.0,0.0)	14.040
3	24	(0.5,0.5,0.5;1.0,0.0,0.0;1.5,0.5,0.5)	0.720
3	24	(0.5,0.5,0.5;1.0,0.0,0.0;1.5,0.5,-0.5)	-13.584
3	24	(0.5,0.5,0.5;1.5,0.5,0.5;1.5,0.5,-0.5)	-8.400
3	16	(0.5,0.5,0.5;0.5,1.5,-0.5;1.5,0.5,-0.5)	1.584
3	48	(0.5,0.5,0.5;0.0,0.0,0.0;0.0,-1.0,0.0)	-35.856
3	96	(0.5,0.5,0.5;1.0,0.0,0.0;0.0,-1.0,0.0)	-29.856
3	48	(0.5,0.5,0.5;5,0.5,-0.5;0.0,-1.0,0.0)	-8.352
3	48	(0.5,0.5,0.5;1.5,-0.5,0.5;0.0,-1.0,0.0)	-4.560
3	24	(0.5,0.5,0.5;-0.5,0.5,-0.5;0.0,-1.0,0.0)	6.600
4	12	(0.5,0.5,0.5;1.0,1.0,0.0;1.0,0.0,0.0;1.5,0.5,0.5)	4.056
4	12	(0.5,0.5,0.5;1.0,1.0,0.0;1.0,0.0,0.0;1.5,0.5,-0.5)	2.532
4	48	(0.5,0.5,0.5;1.0,0.0,0.0;1.5,0.5,0.5;1.5,0.5,-0.5)	1.440
4	6	(0.5,0.5,0.5;0.5,0.5,-0.5;1.5,0.5,0.5;1.5,0.5,-0.5)	2.694
4	16	(0.5,0.5,0.5;1.0,1.0,0.0;0.5,1.5,-0.5;1.5,0.5,-0.5)	-0.752
4	16	(0.5,0.5,0.5;0.5,0.5,-0.5;0.5,1.5,-0.5;1.5,0.5,-0.5)	1.152
4	4	(0.5,0.5,0.5;1.5,1.5,0.5;0.5,1.5,-0.5;1.5,0.5,-0.5)	-2.744
5	24	(0.5,0.5,0.5;1.0,1.0,0.0;1.0,0.0,0.0;1.5,0.5,0.5;1.5,0.5,-0.5)	11.208
5	12	(0.5,0.5,0.5;1.0,0.0,0.0;0.5,0.5,-0.5;1.5,0.5,0.5;1.5,0.5,-0.5)	12.288
5	16	(0.5,0.5,0.5;1.0,1.0,0.0;0.5,0.5,-0.5;0.5,1.5,-0.5;1.5,0.5,-0.5)	-14.592
5	4	(0.5,0.5,0.5;1.0,1.0,0.0;1.5,1.5,0.5;0.5,1.5,-0.5;1.5,0.5,-0.5)	2.856

$a = 3.224\,59\text{ \AA}$, $c = 12.978\,53\text{ \AA}$

Wyckoff positions:

W_1 $1a(0,0,0)$

W_2 $2g(0,0,0.253\,81)$

W_3 $2h(\frac{1}{2},\frac{1}{2},0.372\,61)$

Ta_1 $1b(0,0,\frac{1}{2})$

Ta_2 $2h(\frac{1}{2},\frac{1}{2},0.124\,95)$

W_6Ta_6

Space group: $Cmmm$ (no. 65).

Lattice constants:

$a = 13.791\,83\text{ \AA}$, $b = 3.239\,55\text{ \AA}$, $c = 4.595\,01\text{ \AA}$

Wyckoff positions:

W_1 $2d(0,0,\frac{1}{2})$

W_2 $4g(0.170\,27,0,0)$

Ta_1 $2b(\frac{1}{2},0,0)$

Ta_2 $4h(0.336\,74,0,\frac{1}{2})$

W_5Ta_7

Space group: $P\bar{3}m1$ (no. 164).

Lattice constants:

$a = 4.595\,33\text{ \AA}$, $c = 11.359\,21\text{ \AA}$

$\alpha = 90.00^\circ$, $\beta = 90.00^\circ$, $\gamma = 120.00^\circ$

Wyckoff positions:

W_1 $1a(0,0,0)$

W_2 $2d(\frac{1}{3},\frac{2}{3},0.170\,31)$

W_3 $2d(\frac{1}{3},\frac{2}{3},0.412\,93)$

Ta_1 $1b(0,0,\frac{1}{2})$

Ta_2 $2c(0,0,0.243\,21)$

Ta_3 $2d(\frac{1}{3},\frac{2}{3},0.661\,07)$

Ta_4 $2d(\frac{1}{3},\frac{2}{3},0.919\,09)$

W_4Ta_9

Space group: $I4/m$ (no. 87).

Lattice constants:

$a = 11.828\,13\text{ \AA}$, $c = 3.279\,55\text{ \AA}$

Wyckoff positions:

W_1 $8h(0.538\,18,0.307\,41,0)$

Ta_1 $2a(0,0,0)$

Ta_2 $8h(0.151\,19,0.224\,91,0)$

Ta_3 $8h(0.378\,75,0.074\,30,0)$

W_4Ta_{12}

Space group: $P4_2/mnm$ (no. 136).

Lattice constants:

$a = 9.297\,69\text{ \AA}$, $c = 3.293\,02\text{ \AA}$

Wyckoff positions:

W_1 $4f(0.125\,58,0.125\,58,0)$

Ta_1 $4f(0.380\,08,0.380\,08,0)$

Ta_2 $8i(0.132\,99,0.622\,24,0)$

$W_{15}V$

Space group: $Pm\bar{3}m$ (no. 221).

Lattice constant:

TABLE IX. Many-body effective cluster interactions (in meV) derived for W-V binary alloys

No. of points	m_α	Points in clusters	Symmetry-weighted ECI
0	1		-126.704
1	2	(0,0,0,0,0)	78.528
2	8	(0,0,0,0,0;0.5,0.5,0.5)	91.208
2	6	(0,0,0,0,0;1,0,0,0,0)	34.992
2	12	(0,0,0,0,0;1,0,0,0,-1.0)	8.844
2	24	(0,0,0,0,0;0,0,1,5,0,0)	-19.968
2	8	(0.5,0.5,0.5;1.5,1.5,-0.5)	5.896
2	6	(0,0,0,0,0;0,0,0,2,0)	4.218
2	24	(0,0,0,0,0;1.5,1.5,0.5)	-1.008
2	24	(0,0,0,0,0;-2,1,0,0,0)	-4.224
3	24	(0.5,0.5,0.5;0,0,0,0,0;0.5,0.5,-0.5)	-20.112
3	24	(0.5,0.5,0.5;0,0,0,0,0;0.5,-0.5,-0.5)	-19.656
3	24	(0.5,0.5,0.5;0.5,0.5,-0.5;0.5,-0.5,-0.5)	-12.264
3	16	(0.5,0.5,0.5;-0.5,0.5,-0.5;0.5,-0.5,-0.5)	7.472
3	48	(1.0,1.0,1.0;1.5,1.5,1.5;1.5,1.5,2.5)	-18.480
3	96	(1.0,1.0,1.0;1.5,0.5,1.5;1.5,1.5,2.5)	-22.848
3	48	(1.0,1.0,1.0;2.0,1.0,1.0;1.5,1.5,2.5)	8.352
3	24	(1.0,1.0,1.0;2.0,2.0,1.0;1.5,1.5,2.5)	0.864
3	48	(1.0,1.0,1.0;1.0,-0.2,2.0;1.5,1.5,2.5)	5.808
4	12	(0.5,0.5,0.5;1.0,0,0,0,0;0,0,0,0,0;0.5,0.5,-0.5)	2.772
4	12	(0.5,0.5,0.5;1.0,0,0,0,0;0,0,0,0,0;0.5,-0.5,-0.5)	5.532
4	48	(0.5,0.5,0.5;0,0,0,0,0;0.5,0.5,-0.5;0.5,-0.5,-0.5)	7.824
4	6	(0.5,0.5,0.5;0.5,-0.5,0.5;0.5,0.5,-0.5;0.5,-0.5,-0.5)	2.640
4	16	(0.5,0.5,0.5;0,0,0,0,0;-0.5,0.5,-0.5;0.5,-0.5,-0.5)	-3.952
4	16	(0.5,0.5,0.5;0.5,0.5,-0.5;-0.5,0.5,-0.5;0.5,-0.5,-0.5)	-1.184
4	4	(0.5,0.5,0.5;-0.5,-0.5,0.5;-0.5,0.5,-0.5;0.5,-0.5,-0.5)	-4.384
5	24	(0.5,0.5,0.5;1.0,0,0,0,0;0,0,0,0,0;0.5,0.5,-0.5;0.5,-0.5,-0.5)	8.208
5	12	(0.5,0.5,0.5;0,0,0,0,0;0.5,-0.5,0.5;0.5,0.5,-0.5;0.5,-0.5,-0.5)	6.636
5	16	(0.5,0.5,0.5;0,0,0,0,0;0.5,0.5,-0.5;-0.5,0.5,-0.5;0.5,-0.5,-0.5)	-4.656
5	4	(0.5,0.5,0.5;0,0,0,0,0;-0.5,-0.5,0.5;-0.5,0.5,-0.5;0.5,-0.5,-0.5)	-0.020

$a = 6.35574 \text{ \AA}$
 Wyckoff positions:
 $W_1 1b(\frac{1}{2}, \frac{1}{2}, \frac{1}{2})$
 $W_2 3c(0, \frac{1}{2}, \frac{1}{2})$
 $W_3 3d(\frac{1}{2}, 0, 0)$
 $W_4 8g(0.24847, 0.24847, 0.24847)$
 $V_1 1a(0, 0, 0)$
 W_7V
 Space group: $I4/mmm$ (no. 139).
 Lattice constants:
 $a = 4.47463 \text{ \AA}, c = 12.67978 \text{ \AA}$
 Wyckoff positions:
 $W_1 2b(0, 0, \frac{1}{2})$
 $W_2 4e(0, 0, 0.24912)$
 $W_3 8g(0, \frac{1}{2}, 0.37648)$
 $V_1 2a(0, 0, 0)$
 W_4V
 Space group: $R\bar{3}m$ (no. 166).
 Lattice constants:
 $a = 4.46005 \text{ \AA}, c = 13.65303 \text{ \AA}$
 $\alpha = 90.00^\circ, \beta = 90.00^\circ, \gamma = 120.00^\circ$
 Wyckoff positions:
 $W_1 6c(0, 0, 0.10095)$
 $W_2 6c(0, 0, 0.29974)$
 $V_1 3b(0, 0, \frac{1}{2})$

W_3V
 Space group: $Fm\bar{3}m$ (no. 225).
 Lattice constants:
 $a = 6.28327 \text{ \AA}$
 Wyckoff positions:
 $W_1 4b(\frac{1}{2}, \frac{1}{2}, \frac{1}{2})$
 $W_1 8c(\frac{1}{4}, \frac{1}{4}, \frac{1}{4})$
 $V_1 4a(0, 0, 0)$
 W_2V
 Space group: $I4/mmm$ (no. 139).
 Lattice constants:
 $a = 3.12478 \text{ \AA}, c = 9.34678 \text{ \AA}$
 Wyckoff positions:
 $W_1 4e(0, 0, 0.33542)$
 $V_1 2a(0, 0, 0)$
 W_3V_2
 Space group: $R\bar{3}m$ (no. 166).
 Lattice constants:
 $a = 4.39348 \text{ \AA}, c = 13.50491 \text{ \AA}$
 $\alpha = 90.00^\circ, \beta = 90.00^\circ, \gamma = 120.00^\circ$
 Wyckoff positions:
 $W_1 3a(0, 0, 0)$
 $W_2 6c(0, 0, 0.20068)$
 $V_1 6c(0, 0, 0.39889)$

W_2V_2
 Space group: $Fd\bar{3}m$ (no. 227).
 Lattice constants:
 $a = 6.19440 \text{ \AA}$
 Wyckoff positions:
 $W_1 8a(\frac{1}{8}, \frac{1}{8}, \frac{1}{8})$
 $V_1 8b(\frac{3}{8}, \frac{3}{8}, \frac{3}{8})$
 W_2V_3
 Space group: $R\bar{3}m$ (no. 166).
 Lattice constants:
 $a = 4.33170 \text{ \AA}$, $c = 13.40091 \text{ \AA}$
 $\alpha = 90.00^\circ$, $\beta = 90.00^\circ$, $\gamma = 120.00^\circ$
 Wyckoff positions:
 $W_1 6c(0,0,0.20068)$
 $V_1 3b(0,0,\frac{1}{2})$
 $V_2 6c(0,0,0.39889)$
 W_3V_5
 Space group: $R\bar{3}m$ (no. 166).

Lattice constants:
 $a = 4.30712 \text{ \AA}$, $c = 21.60209 \text{ \AA}$
 $\alpha = 90.00^\circ$, $\beta = 90.00^\circ$, $\gamma = 120.00^\circ$
 Wyckoff positions:
 $W_1 3a(0,0,0)$
 $W_2 6c(0,0,0.12450)$
 $V_1 3b(0,0,\frac{1}{2})$
 $V_2 6c(0,0,0.24957)$
 $V_3 6c(0,0,0.37413)$
 W_3V_{12}
 Space group: $R\bar{3}m$ (no. 166).
 Lattice constants:
 $a = 4.29264 \text{ \AA}$, $c = 13.17394 \text{ \AA}$
 $\alpha = 90.00^\circ$, $\beta = 90.00^\circ$, $\gamma = 120.00^\circ$
 Wyckoff positions:
 $W_1 3a(0,0,0)$
 $V_1 6c(0,0,0.19843)$
 $V_2 6c(0,0,0.40095)$

*duc.nguyen@ccfe.ac.uk

- ¹M. Rieith, J. L. Boutard, S. L. Dudarev, T. Ahlgren, S. Antusch, N. Baluc, M.-F. Barthe, C. S. Becquart, L. Ciupinski, J. B. Correia, C. Domain, J. Fikar, E. Fortuna, C.-C. Fu, E. Gaganidze, T. L. Galàn, C. García-Rosales, B. Gludovatz, H. Greuner, K. Heinola, N. Holstein, N. Juslin, F. Koch, W. Krauss, K. J. Kurzydłowski, J. Linke, C. Linsmeier, N. Luzginova, H. Maier, M. S. Martínez, J. M. Missiaen, M. Muhammed, A. Munoz, M. Muzyk, K. Nordlund, D. Nguyen-Manh, P. Norajitra, G. Pintsuk, R. Pippan, G. Ritz, L. Romaner, D. Rupp, R. Schäublin, J. Schlosser, I. Uytdenhouten, J. G. van der Laan, L. Veleva, L. Ventelon, S. Wahlberg, F. Willaime, S. Wurster, and M. A. Yar, *J. Nucl. Mater.*, doi: [10.1016/j.jnucmat.2011.01.075](https://doi.org/10.1016/j.jnucmat.2011.01.075).
- ²J. Pamela, A. Bécoulet, D. Borba, J.-L. Boutard, L. Horton, and D. Maisonnier, *Fusion Eng. Des.* **84**, 194 (2009).
- ³P. Norajitra, S. I. Abdel-Khalik, L. M. Giancarli, T. Ihli, G. Janeschitz, S. Malang, I. V. Mazul, and P. Sardain, *Fusion Eng. Des.* **83**, 893 (2008).
- ⁴H. Bolt, V. Barabash, W. Krauss, J. Linke, R. Neu, S. Suzuki, and N. Yoshida, *J. Nucl. Mater.* **329–333**, 66 (2004).
- ⁵T. Hirai, G. Pintsuk, J. Linke, and M. Batilliot, *J. Nucl. Mater.* **390–391**, 751 (2009).
- ⁶J. Roth, E. Tsitrona, A. Loarte, Th. Loarer, G. Counsell, R. Neu, V. Philipps, S. Brezinsek, M. Lehnen, P. Coad, Ch. Grisolia, K. Schmid, K. Krieger, A. Kallenbach, B. Lipschultz, R. Doerner, R. Causey, V. Alimov, W. Shu, O. Ogorodnikova, A. Kirschner, G. Federici, A. Kukushkin, and EFDA PWI Task Force, ITER PWI Team, Fusion for Energy, ITPA SOL/DIV, *J. Nucl. Mater.* **390**, 1 (2009).
- ⁷A. Giannattasio and S. G. Roberts, *Philos. Mag.* **87**, 2589 (2007).
- ⁸H. Kurishitai, S. Matsuo, H. Arakawa, M. Narui, M. Yamazaki, T. Sakamoto, S. Kobayashi, K. Nakai, T. Takida, K. Tabeke, M. Kawai, and N. Yoshida, *J. Nucl. Mater.* **386**, 579 (2009).
- ⁹S. Zinkle and N. Ghoniem, *Fusion Eng. Des.* **49**, 709 (2000).
- ¹⁰P. L. Raffo, *J. Less-Common Met.* **17**, 133 (1969).
- ¹¹W. D. Klopp, *J. Less-Common Met.* **42**, 261 (1975).
- ¹²Y. Mutoh, K. Ichikawa, K. Nagata, and M. Takeuchi, *J. Mater. Sci.* **30**, 770 (1995).
- ¹³L. Romaner, C. Ambrosch-Draxl, and R. Pippan, *Phys. Rev. Lett.* **104**, 195503 (2010).
- ¹⁴I. Smid, N. Akiba, G. Vieider, and L. Ploch, *J. Nucl. Mater.* **258–263**, 160 (1998).
- ¹⁵C. B. A. Forty, C. J. Butterworth, and J.-Ch. Sublet, *J. Nucl. Mater.* **212–215**, 640 (1994).
- ¹⁶T. Noda, M. Fujita, and M. Okada, *J. Nucl. Mater.* **258–263**, 934 (1998).
- ¹⁷G. A. Cottrell, *J. Nucl. Mater.* **334**, 166 (2004).
- ¹⁸M. R. Gilbert and J. C. Sublet, *Nucl. Fus.* **51**, 043005 (2011).
- ¹⁹S. V. Nagender Naidu, A. M. Sriramamurthy, M. Vijayakumar, and P. Rama Rao, “V-W (*Vanadium-Tungsten*),” *Phase Diagrams of Binary Vanadium Alloys*, edited by J. E. Smith (ASM International, Materials Park, OH, 1989), pp. 313–317.
- ²⁰*Binary Alloy Phase Diagrams*, edited by T. B. Massalski (ASM International, Materials Park, OH, 1990).
- ²¹*Binary Systems from Mn-Mo to Y-Zr, Band 17, Teil 4, Landolt-Bornstein: Numerical Data and Functional Relationships in Science and Technology, New Series*, compiled by Scientific Group Thermodata Europe (SGTE), Springer Verlag (2006).
- ²²S. C. Singhal and W. L. Worrell, *Metall. Trans.* **4**, 895 (1973).
- ²³P. E. A. Turchi, V. Drchal, J. Kudrnovsky, C. Colinet, L. Kaufman, and Z.-K. Liu, *Phys. Rev. B* **71**, 094206 (2005).
- ²⁴V. Blum and A. Zunger, *Phys. Rev. B* **72**, 020104 (2005).
- ²⁵G. L. W. Hart, V. Blum, M. J. Walorski, and A. Zunger, *Nat. Mater.* **4**, 391 (2005).
- ²⁶C. Colinet and A. Pasturel, *Physica B* **159**, 275 (1989).
- ²⁷C. Sigli and J. M. Sanchez, *Acta Metall.* **36**, 367 (1988).
- ²⁸D. Nguyen-Manh, A. P. Horsfield, and S. L. Dudarev, *Phys. Rev. B* **73**, 020101(R) (2006).
- ²⁹D. Nguyen-Manh, S. L. Dudarev, and A. P. Horsfield, *J. Nucl. Mater.* **367–370**, 257 (2007).
- ³⁰P. M. Derlet, D. Nguyen-Manh, and S. L. Dudarev, *Phys. Rev. B* **76**, 054107 (2007).
- ³¹M. R. Gilbert, S. L. Dudarev, P. M. Derlet, and D. G. Pettifor, *J. Phys.: Condens. Matter* **20**, 345214 (2008).
- ³²D. Nguyen-Manh, *Adv. Mater. Res.* **59**, 253 (2009).

- ³³ *Materials Subjected to Fast Neutron Irradiation*, edited by J.-L. Boutard and S. L. Dudarev, *C. R. Phys.* **9**, 285 (2008).
- ³⁴ J. Hole, P. Gumbsch, *J. Nucl. Mater.* **400**, 218 (2010).
- ³⁵ S. Wurster, B. Gludovatz, A. Hoffmann, and R. Pippan, *J. Nucl. Mater.* **413**, 166 (2011).
- ³⁶ J. M. Sanchez, F. Ducastelle, and D. Gratias, *Physica A* **128**, 334 (1984).
- ³⁷ A. Zunger, in *NATO Advanced Study Institute on Statics and Dynamics of Alloy Phase Transformations*, NATO Advanced Study Institute Vol. 319, edited by P. E. Turchi and A. Gonis (Plenum, New York, 1994), p. 361.
- ³⁸ D. de Fontaine, *Solid State Phys.* **47**, 33 (1994).
- ³⁹ A. van de Walle, *Calphad* **33**, 266 (2009).
- ⁴⁰ D. Nguyen-Manh, M. Y. Lavrentiev, and S. L. Dudarev, *J. Computer-Aided Mater. Des.* **14**, 159 (2007).
- ⁴¹ M. Y. Lavrentiev, R. Drautz, D. Nguyen-Manh, T. P. C. Klaver, and S. L. Dudarev, *Phys. Rev. B* **75**, 014208 (2007).
- ⁴² D. Nguyen-Manh, M. Y. Lavrentiev, and S. L. Dudarev, *C. R. Phys.* **9**, 379 (2008).
- ⁴³ J. P. Perdew, K. Burke, and M. Ernzerhof, *Phys. Rev. Lett.* **77**, 3865 (1996).
- ⁴⁴ G. Kresse and J. Hafner, *Phys. Rev. B* **47**, 558 (1993).
- ⁴⁵ G. Kresse and J. Furthmüller, *Phys. Rev. B* **54**, 11169 (1996).
- ⁴⁶ G. Kresse and D. Joubert, *Phys. Rev. B* **59**, 1758 (1999).
- ⁴⁷ J. W. D. Connolly and A. R. Williams, *Phys. Rev. B* **27**, 5169 (1983).
- ⁴⁸ A. Zunger, S. H. Wei, L. G. Ferreira, and J. E. Bernard, *Phys. Rev. Lett.* **65**, 353 (1990).
- ⁴⁹ M. L. Jokl, V. Vitek, and C. J. McMahon Jr., *Acta Metall.* **28**, 1479 (1980).
- ⁵⁰ D. G. Pettifor, *Bonding and Structure of Molecules and Solids* (Oxford, Clarendon, 1995).
- ⁵¹ L. Kaufman, P. E. A. Turchi, W. Huang, and Z.-K. Liu, *Calphad* **25**, 419 (2001).
- ⁵² N. Saunders and A. P. Miodownik, *CALPHAD: A Comprehensive Guide*, Pergamon Materials Series (Oxford, New York, 1998).
- ⁵³ I. M. Neklyudov, E. V. Sadanov, G. D. Tolstolutskaia, V. A. Ksenofontov, T. I. Mazilova, and I. M. Mikhailovskij, *Phys. Rev. B* **78**, 115418 (2008).
- ⁵⁴ K. Arakawa, K. Ono, M. Isshiki, K. Mimura, M. Uchikoshi, and H. Mori, *Science* **318**, 956 (2007).
- ⁵⁵ T. Amiro, K. Arakawa, and H. Mori, *Philos. Mag. Lett.* **91**, 86 (2011).
- ⁵⁶ D. Nguyen-Manh, M. Muzyk, K. J. Kurzydłowski, N. L. Baluc, M. Reith, and S. L. Dudarev, *Key Eng. Mater.* **465**, 15 (2011).
- ⁵⁷ H. Eleveld and A. van Veen, *J. Nucl. Mater.* **212–215**, 1421 (1994).
- ⁵⁸ P. E. Lhuillier, M. F. Barthe, P. Desgardin, W. Egger, and P. Sperr, *Phys. Status Solidi C* **6**, 2329 (2009).
- ⁵⁹ M. F. Barthe (private communication).
- ⁶⁰ C. S. Becquart and C. Domain, *Nucl. Instrum. Methods Phys. Res. B* **255**, 23 (2007).
- ⁶¹ C. S. Becquart and C. Domain, *J. Nucl. Mater.* **385**, 223 (2009).
- ⁶² C. S. Becquart, C. Domain, U. Sarkar, A. DeBacker, and M. Hou, *J. Nucl. Mater.* **403**, 75 (2010).
- ⁶³ J. P. Perdew, J. A. Chevary, S. H. Vosko, K. A. Jackson, M. R. Pederson, and C. Fiolhais, *Phys. Rev. B* **46**, 6671 (1992).
- ⁶⁴ L. Ventelon, F. Willaime, C.-C. Fu, M. Heran, and I. Ginoux, *J. Nucl. Mater.* (unpublished).
- ⁶⁵ R. Armiento and A. E. Mattsson, *Phys. Rev. B* **72**, 085108 (2005).
- ⁶⁶ D. Kato, H. Iwariki, and K. Morishita, *J. Nucl. Mater.*, doi: 10.1016/j.jnucmat.2010.12.211.
- ⁶⁷ J. Y. Park, H. C. W. Huang, R. W. Siegel, and R. W. Balluffi, *Philos. Mag. A* **48**, 397 (1983).
- ⁶⁸ K.-H. C. Lie and J. S. Koehler, *Adv. Phys.* **17**, 421 (1968).
- ⁶⁹ T. S. Hudson, S. L. Dudarev, M. J. Caturla, and A. P. Sutton, *Philos. Mag.* **85**, 661 (2004).
- ⁷⁰ S. L. Dudarev, P. M. Derlet, and R. Bullough, *J. Nucl. Mater.* **386–388**, 45 (2009).
- ⁷¹ T. Ahlgren, K. Heinola, N. Juslin, and A. Kuronen, *J. Appl. Phys.* **107**, 033516 (2010).
- ⁷² T. S. Hudson, S. L. Dudarev, and A. P. Sutton, *Proc. R. Soc. London Ser. A* **460**, 2457 (2004).
- ⁷³ S. L. Dudarev, M. R. Gilbert, K. Arakawa, H. Mori, Z. Yao, M. L. Jenkins, and P. M. Derlet, *Phys. Rev. B* **81**, 224107 (2010).
- ⁷⁴ P. Olsson, T. P. C. Klaver, and C. Domain, *Phys. Rev. B* **81**, 054102 (2010).
- ⁷⁵ C. E. Anderson and F. R. Brotzen, *J. Appl. Phys.* **53**, 292 (1982).
- ⁷⁶ D. E. J. Armstrong, A. J. Wilkinson, and S. G. Roberts, *J. Mater. Res.* **24**, 3268 (2009).
- ⁷⁷ A. Kelly, W. Tyson, and A. H. Cottrell, *Philos. Mag.* **15**, 567 (1967).
- ⁷⁸ J. R. Rice and R. Thompson, *Philos. Mag.* **29**, 78 (1974).